Monte Carlo Simulation of Neutron Shielding for Proton Therapy Facilities

by

Michael R. Folkert

SUBMITTED TO THE DEPARTMENT OF NUCLEAR ENGINEERING IN PARTIAL FULFILLMENT OF THE REQUIREMENTS FOR THE DEGREES OF

BACHELOR OF SCIENCE IN NUCLEAR ENGINEERING
AND
MASTER OF SCIENCE IN NUCLEAR ENGINEERING
AT THE
MASSACHUSETTS INSTITUTE OF TECHNOLOGY

JUNE 1998

Signature of Author: _____
Department of Nuclear Engineering
May 8, 1998

Certified by: _____
Jacquelyn C. Yanch
Associate Professor of Nuclear Engineering
Thesis Supervisor

_____
Wayne D. Newhauser
Instructor in Radiation Oncology, Harvard Medical School
Thesis Reader

Accepted by: _____
Lawrence M. Lidsky
Professor of Nuclear Engineering
Chairman, Department Committee on Graduate Students

Monte Carlo Simulation of Neutron Shielding for Proton Therapy Facilities

by

Michael R. Folkert

Submitted to the Department of Nuclear Engineering
on May 8, 1998 in Partial Fulfillment of the
Requirements for the Degrees of Bachelor of Science and
Master of Science in Nuclear Engineering

ABSTRACT

A study was performed to develop a Monte Carlo method of modeling neutron shielding of proton therapy facilities in a complex, realistic environment. The bulk neutron shielding of the Northeast Proton Therapy Center (Massachusetts General Hospital, Boston, MA) was used as the basis of the design work. A geometrical model of the facility was simulated using the LAHET Code System, a set of Monte Carlo codes developed at Los Alamos National Laboratory. Additional software tools for reading and analyzing the simulation data that the model provides have been developed and tested. In order to verify the computer simulations, neutron detection and data acquisition systems have been assembled, modified, and thoroughly tested in order to monitor the neutron dose equivalent during proton beam operation at several locations on a continuous basis. Preliminary tests show that the geometry and physics models proposed in this work are valid.

Thesis Supervisor: Jacquelyn C. Yanch
Title: Associate Professor of Nuclear Engineering

Acknowledgments

I wish to acknowledge the support of the Massachusetts Institute of Technology Nuclear Engineering Department and of the INPO, and I thank them for the financial assistance I have received while I have been involved in this project. I would like to thank my advisor, Dr. Jacquelyn Yanch, for her advice, commentary, and support during the course of this work.

In the course of this study, I have been assisted by many people, whithout whom this project could not have been completed. My supervisor at the Northeast Proton Therapy Center, Dr. Wayne Newhauser, deserves the greatest recognition, having been an inexhaustible source of information and guidance for the past year, and I look forward to continue my research with him in the future. Yves Jongen and the staff of Ion Beam Applications have been very helpful in supplying proton beam time. Steve Bradley of NPTC and the Bechtel Corporation graciously provided the blueprints and concrete information used in the simulations. I would also like to thank Dr. Alfred Smith for his assistance in providing the computing resources necessary for the development of this work. Michelle Ledesma has lent me her eye for detail and her enthusiasm for seeing a project through - I couldn't ask for a better friend.

My parents deserve more thanks than I could possibly give for their unflagging support in helping me get through all these years at MIT. Their faith in me has been the sustaining force behind my efforts, and they have been behind me all of the way. I would like to thank Julie Anne Mason, for without her love, support, and understanding I would have killed myself with a rock weeks ago. To all my friends and everyone else who have helped me along the way, I love you all, and thanks.

Table of Contents

List of Tables and Figures

Tables

Figures

SECTION 1 - INTRODUCTION

Proton therapy is a radiotherapy modality that uses beams of high-energy protons to deliver a tightly-constrained amount of energy to a specified target volume in order to selectively destroy tumor cells with minimal deleterious effect on surrounding healthy tissue. In the course of producing and delivering high-energy proton beams, a significant radiological hazard is introduced by neutrons that are generated as a result of protons undergoing nuclear interactions with materials in the beam path. These neutrons are the dominant secondary radiation field in proton therapy and shielding must be designed to protect the workers in close proximity to the therapy equipment and the general public.

Larson et al.[28] designed the radiation shielding for the Northeast Proton Therapy Center (NPTC), located on the Massachusetts General Hospital (MGH) campus in Boston, using a variety of analytical techniques. The shielding design is a complex and difficult engineering task that is not easily modeled with analytical methods. In most cases, previous shielding calculations have followed a simplified approach in which the energy and angular distributions of secondary neutrons produced by proton beam interactions are calculated and then transported through a concrete shield wall. The energy and angular distributions of the attenuated neutrons are then calculated at several depths in the concrete, and the neutron dose equivalent is calculated from these distributions.[1,2,9,30,50] For a single-source situation with a simple flat or spherical wall surrounding it, these approximations are sufficient. However, these methods can at best approximately model the complexity introduced by multiple sources interacting with multiple neutron shielding barriers, as is the case in a multi-purpose proton therapy facility capable of producing and delivering proton beams with a wide range of energies to a variety of locations and targets.

It is the goal of this work to develop more accurate methods for predicting shielding performance. Specifically, an existing Monte Carlo code is being modified and supplemented with additional computer codes that allow the simulation of neutron

shielding in a complex, realistic geometry. Towards this end, a computer model of the Northeast Proton Therapy Center's bulk neutron shielding geometry has been created. In addition, neutron dosimetry instrumentation has been developed for confirmatory measurements. These instruments will provide experimental verification of the shielding performance at NPTC once the beam delivery systems and beamline instrumentation are fully operational.

The simulation of the NPTC shielding and the software tools developed in this work are expected to yield great potential benefits for future work in proton therapy, as these calculational tools can be applied to the optimization of neutron shielding designs for future facilities. This may allow future designers to use less shielding material and as a result reduce the cost of the construction of new facilities. Any reduction in the size of the shielding walls will also free up floor space, which is especially important in urban areas where the cost of the land for the facility can be a significant fraction of the total cost.

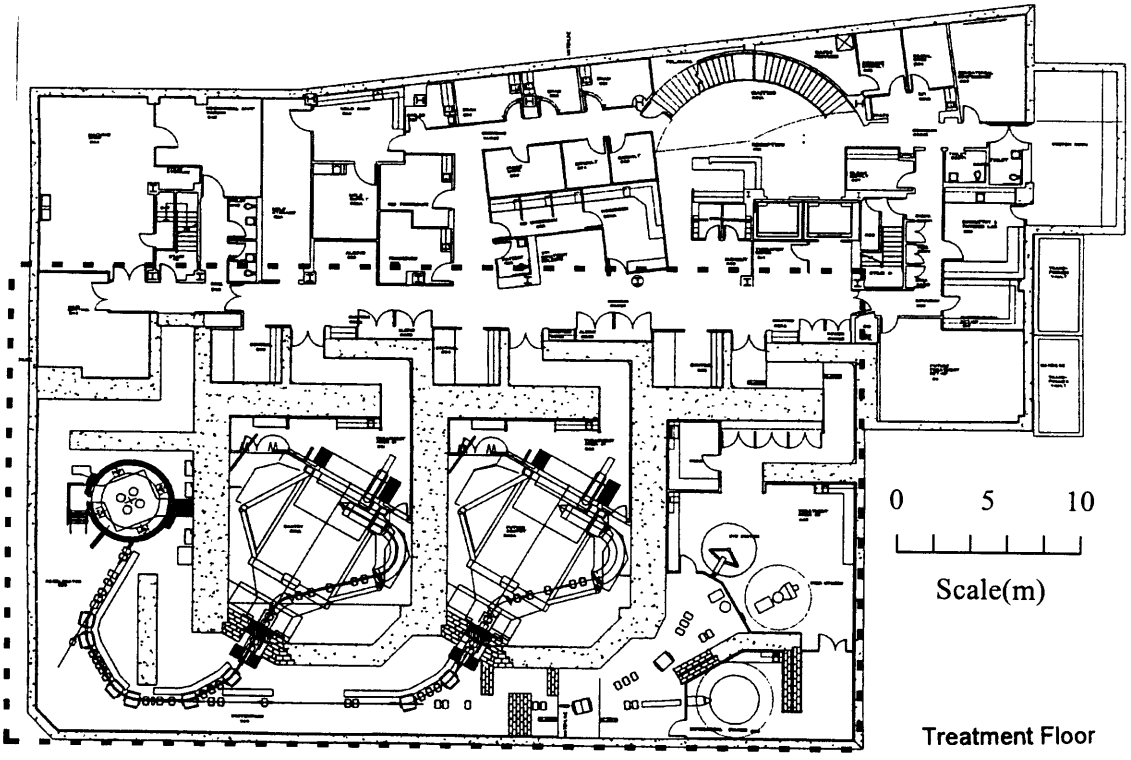

Figure 1.1. Layout of the treatment floor of the Northeast Proton Therapy Center.

Figure 1.1 illustrates the layout of the NPTC treatment floor.[7] The focus of the computer model is the 3-dimensional region within the dashed box, which contains all of the neutron shielding barriers (the dotted regions) and the beam delivery components, i.e., the accelerator, energy degrader, bending/focusing magnets, and patient positioning system.

This work is organized as follows:

- Section 2 provides background information on how the neutron fields are produced by the proton beam interactions with materials in the beam transport components and with the patient.
- Section 3 describes pertinent characteristics of the Northeast Proton Therapy Center, the general specifications for the neutron shielding in terms of the neutron sources, regulatory limits on dose equivalent, and factors that influence the choice of shielding material.
- Section 4 provides information on Monte Carlo techniques for radiation transport simulations and on the Los Alamos High Energy Transport Code (LAHET), the Monte Carlo code that was chosen for the NPTC simulations.
- Section 5 covers the Monte Carlo calculation methods for the simulation of NPTC, including a detailed geometrical model of the neutron shielding barriers, the determination of the neutron source terms, the characterization of the materials, the development of new codes to process the massive amount of data generated in the course of the LAHET calculations, and how best to interpret the simulation results.
- Section 6 describes a measurement system for experimentally verifying the LAHET predictions of neutron dose equivalent.
- Section 7 presents the conclusions of this work and illustrates the potential applications this study may have in the design of future proton therapy facilities.

SECTION 2 - BACKGROUND

In predicting the radiological hazards presented by the clinical operation of a proton accelerator, the means by which neutrons are produced must be taken into account. The neutron production reactions that protons undergo in various target materials is dependent both on the incident proton energy and/or the characteristics of the target nuclei. Different proton-induced nuclear reactions result in widely different resulting neutron radiation fields, and accurate neutron dose equivalent determination requires detailed information on the characteristics of these fields. This necessitates the use of models that adequately predict the radiation fields expected during normal clinical operation of the accelerator.

2.1 Proton Beams

For the last 75 years, radiation has been used to non-invasively treat malignant tumors in living tissue. First proposed by Wilson[61] in 1946 and implemented in 1957,[49] high energy protons have augmented the armamentarium of radiation 'modalities,' initially constrained to gamma rays, x rays, and electrons, used to selectively irradiate cancerous tissue.[38] The primary motivating factor for the clinical use of these widely differing modalities has been to improve control over the deposition of therapeutic dose.[29] Sources of electromagnetic radiation, such as x rays or gamma rays, deposit energy over an extended region, i.e., proximal and distal to the target volume, even with the most precise restraint on the beams' spread in the lateral directions. Electrons are easily scattered and their directionality is poorly constrained. High-energy proton beams, on the other hand, have very different physical characteristics. Protons of a given energy penetrate a finite distance into the patient, and then come to rest. The range of protons in water is described in Equation 2.1, which corresponds to physical data for the proton energy range from 100 to 250 MeV[6]

$$R_i = (2.63x10^{-3})x(E_i)^{1.74}(\,^{g}/_{cm^2}) \qquad (2.1)$$

where R_i is the range of the incident proton and E_i is its associated energy in MeV. Equation 2.1 is known as the "range-energy relation." This pattern energy deposition characteristic of proton beams is known as a Bragg Curve, and an example is shown in Figure 2.1.

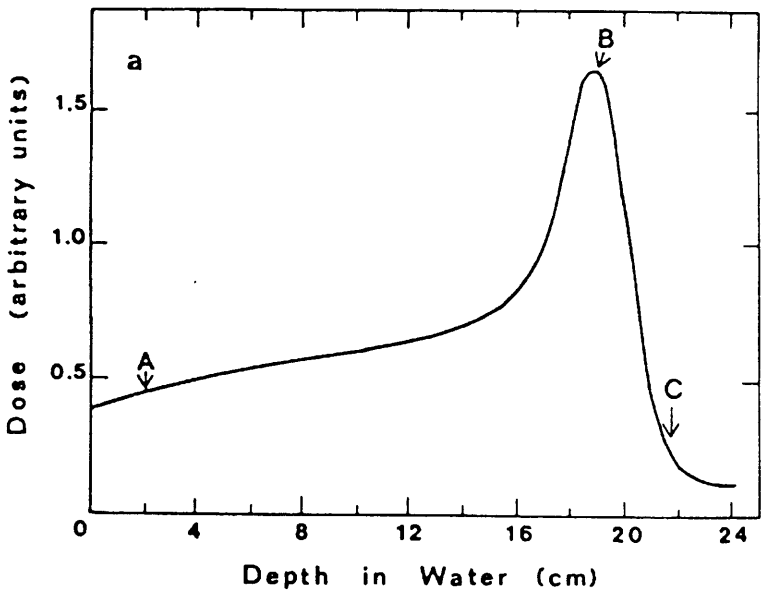

Figure 2.1. Dose-depth plot for 170 MeV protons in water.[65]

Point A in Figure 2.1 is in the region of the Bragg Curve where the incident proton is still fairly energetic and the rate of energy loss is small. The rate of energy deposition increases as the proton loses energy, reaching a maximum at the "Bragg peak."(Point B) After this localized maximum, the proton energy loss rate falls off rapidly (Point C). During the course of the proton's penetration, its greatest energy deposition rate, and consequently its dose rate, is near the Bragg peak. Thus, when protons are directed at a tumor they deliver virtually no dose beyond it, and less dose than x-rays or electrons proximal to it. This can lead to very favorable dose distributions which may allow more dose to be delivered to the tumor while sparing the surrounding healthy tissues.[52] Many of

the tumors that require radiotherapy are located near critical structures (organs that are particularly radiosensitive, such as the central nervous system or the lungs) the use of heavy charged particles such as protons as a treatment modality has proven advantages.[29,52]

In order to treat locations deep within human tissue, a means of producing protons of sufficient energy must be available. Starting in 1962, the Harvard Cyclotron Laboratory (Cambridge) proton synchrocyclotron has been a valuable resource for this proton technology, providing proton beams for Massachusetts General Hospital that have been used to treat over 7000 patients. Its original design energy was about 140 MeV.[38] In order to be able to deliver a dose to any region of the human body, a mean proton beam energy of around 235 MeV is required. A proton beam of 235 MeV gives a range of about 34 cm in water, which allows the irradiation of even a very thick patient from any angle in a plane perpendicular to the patient's longitudinal axis. Such a beam is available at the Loma Linda University Medical Center (San Bernadino, CA), and will soon be available for clinical use at the Northeast Proton Therapy Center (MGH - Boston, MA).[38]

2.2 Neutron Sources

The principal concern in shielding medical proton accelerators is to attenuate the neutron radiation field produced by the (p,xn) reactions in the beam transport components, the accelerator structure, the energy selection system, and the patient to a level within regulatory limits.[57] The estimation of shielding for proton accelerators requires a detailed understanding of the production of particles by the interaction of the primary protons, their transport through the shield and the determination of the energy spectrum of the radiations that escape from the shield. In the energy ranges used clinically at NPTC (70-235 MeV), these calculations are made even more difficult by the rapid changes in hadron cross-sections with energy, and the large differences in neutron yields resulting from these interactions. For example, 70 MeV protons incident on a copper target produce on average 5.5×10^{-2} neutrons per incident proton, while 200 MeV protons produce on average 1 neutron per incident proton, almost a twenty-fold difference in neutron yield.[54]

The neutrons in the treatment rooms result primarily from production within the beam scattering system in the nozzle, the defining aperture, and the patient. The intensity of the neutron field is dependent on the energy and current of the delivered proton beam. The neutron radiation field around the proton beam transport system is primarily due to proton interactions with the beamline components, such as the bending and focusing magnets. The neutron radiation field associated with the energy selection system is due to the proton-induced nonelastic nuclear reactions in the variable thickness graphite energy degrader wheel. A diagram locating these components is provided in Section 3.2.1.

The proton source intensity to be utilized must be specified before any shield design is attempted. In many cases this specification will be straightforward - such as, for example, where a single proton beam utilizes only one beam stop. When multiple beam operation is planned, as is the case at the Northeast Proton Therapy Center, the specification of the source term becomes much more difficult to estimate. The intensity of the neutron beam may vary from treatment to treatment, and an upper limit to the proton beam intensity may be necessary to insure that the dose to the patient can be safely controlled. MGH took these considerations into account when they specified a limit on the maximum proton current the accelerator could produce to 300 nA, approximately one-fifth of the accelerator's maximum output.

2.2.1 Particle Yields from Proton-Nucleus Interactions

For all target materials at primary proton energies E between 50 MeV and 500 MeV, the neutron yield is roughly proportional to the total proton energy squared, E^2. According to Puppi and Dalaporta[47]:

$$\frac{N}{P} = \frac{E^2}{E^2 - (m_0 c^2)^2} \qquad (2.1)$$

Where $\frac{N}{P}$ is the neutron yield per incident proton ratio, E is the proton total energy, and m_0c^2 is the proton rest mass.

For detailed calculations for radiation protection, more than just the number of neutrons produced is required: in particular, the energy and angular distribution of the neutrons must be known. The quantities are needed because the quality factor for neutron dose equivalent determination, **Q**, is a function of neutron energy, and the angular distribution is needed to examine the effects of multiple barriers in a 3-dimensional system. Two nuclear processes that are of particular importance in determining the yield of particles following proton-nucleus interactions: nuclear evaporation and intranuclear cascade.

2.2.2 Nuclear Evaporation

Neutron evaporation is summarized by a two-step model, consisting of the formation of a compound nucleus followed by particle emission and de-excitation. This compound nucleus is in an excited state with a number of allowed decay channels; the preferred decay channel is most energetically favorable, i.e., the entrance channel. As the energy of the incident particle increases, the number of levels available in the incident channel becomes very large; there are no longer discrete levels in the quasi-stationary states of the compound nucleus but rather a complete overlapping of levels inside the nucleus. Under these conditions the emission of particles is best described by an evaporation process analogous to the evaporation of a molecule from the surface of a liquid.[57] The energy distribution of emitted neutrons can be described by a Maxwellian distribution of the form:

$$n(E)dE = cEe^{\frac{-E}{\tau}} \qquad (2.2)$$

where $n(E)$ is the number of neutrons emitted at energy **E** (in MeV), dE is the energy interval, τ is a so-called nuclear temperature and has the dimensions of energy in MeV, and **c** is a constant specific to the system.[55] Similar equations describe the emission of protons, deuterons, and heavier charged particles, but at clinically relevant proton energies these do not influence shielding considerations because their ranges are at most a few centimeters. The evaporated particles are emitted isotropically, and the energy distribution of the evaporated neutrons extends up to about 8 MeV.[54]

2.2.3 Intranuclear Cascade

At higher proton energies (above about 50 MeV) the development of an intranuclear cascade becomes important. The intranuclear cascade develops through an interaction of individual nucleons inside the nucleus; the probability of these interactions is determined by the free nucleon cross-sections and by the Pauli exclusion principle.[4,12,34] These neutrons are emitted preferentially in the forward direction (with respect to the incident proton direction), and by definition may have energies ranging from 8 MeV up to about the incident proton energy.[54]

The number of neutrons per unit energy per solid angle per interaction (cascade or evaporation) of a proton of kinetic energy E_o MeV can be represented by:

$$n(E) = \frac{1}{E_0}\exp\left|\sum_{i=0}^{5} a_i \left|\frac{E}{E_0}\right|^i\right| + \frac{1}{4\pi}\frac{1}{25}\exp\left|\sum_{j=0}^{4} a_j \left|\frac{E}{25}\right|^j\right| \qquad (2.3)$$

where the first term refers to the yield from the intranuclear cascade and the second term refers to the yield from evaporation. The coefficients a_i and a_j are given so that the energy

distributions for both evaporation and cascade neutrons and for each angular region may be calculated.[57]

2.3 Neutron Radiation Fields

The prompt radiation of particle accelerators exists only while they are in operation. As described above, this radiation field may result as a natural consequence of the acceleration process and the utilization of the accelerated beam. The most complex radiation environments around particle accelerators will generally arise at locations where the shielding is 'thin,' i.e., insufficient to fully attenuate the charged particles produced by primary proton-induced nuclear reactions. This situation dominates inside the main shielding barriers. Before interacting, the accelerated beam is basically monoenergetic and of one particle type. Passage through the accelerator structure, experimental equipment or thin shielding will lead to the partial development of electromagnetic and hadronic cascades and the production of many types of particles distributed over a wide range of energies. Outside the main shielding barriers, the situation is simplified. Despite the large variety of high energy particle accelerators, both with respect to beam characteristics and utilization, their external radiation environments outside the shields are often quite similar, and are usually dominated by neutrons ranging in energy from thermal up to about the proton energy (235 MeV for NPTC).[16,17]

2.4 Dosimetry

One of the most important aspects of radiation protection dosimetry at particle accelerators is the interpretation of measurements in terms of the particular dose equivalent quantities required by regulation and statute. The quantity 'dose equivalent' was first formally defined as recently as 1968,[24] although its origins go back a further twenty years to the application of relative biological effectiveness (RBE) dose to radiological protection.[39] Thomas has reviewed the long-standing discussion concerning

the definition of both the quantity and its units.[56] For sources of radiation exposure external to the body, the dose equivalent H is defined by the equation:

$$H = \int_0^{\infty} Q(L_\infty) \frac{dD(L_\infty)}{dL_\infty} dL_\infty \qquad (2.4)$$

Where L_∞ is the unrestricted linear collision stopping power in water, $\frac{dD(L_\infty)}{dL_\infty}$ is the absorbed dose in the stopping power increment from L_∞ to $(L_\infty + dL_\infty)$, $Q(L_\infty)$ is the quality factor as a function of stopping power as defined by ICRU and ICRP,[20,24] and the integral of equation 2.2 is evaluated over the entire L_∞ spectrum.

The primary limits for radiation exposure recommended by the ICRP are expressed in terms of the dose equivalent to various tissues H_t, the whole body dose equivalent H_{wb}, and the effective dose equivalent H_E. For external radiation exposure, secondary limits are expressed in terms of the shallow and deep dose equivalent indexes $H_{I,s}$ and $H_{I,d}$.[20] Since, in general, neither the primary nor the secondary limits may be measured directly, operational quantities were developed.[19,22,23,60]

The most widely used operational dose equivalent quantity for neutrons is the dose equivalent H_c, determined from the measured neutron fluence Φ_m, and a fluence-to-dose-equivalent conversion coefficient h. The coefficient h stands for h(E), expressed in units of dose equivalent per unit fluence. Use of these conversion coefficients requires that the irradiated volume be large enough that the mean chord length is greater than the mean free path of the most penetrating secondary charged particles that are generated by neutron interactions in the target volume.[65] The dose equivalent for monoenergetic neutrons is then

$$H_c = h\Phi_m \qquad (2.5)$$

For polyenergetic neutrons, the equation becomes

$$H_c(E) = h(E)\Phi_m(E) \qquad (2.6)$$

The fluence-to-dose conversion coefficients from the United States Nuclear Regulatory Commission are given below in Table 2.1.[58] These conversion coefficients are appropriate when the mean free paths of the secondary neutrons originally engendered by the proton beam are much longer than those of the tertiary charged particles produced by neutron interactions in the target, and when the target is sufficiently large compared to the mean free paths of these tertiary charged particles.[65]

Neutron Energy, E (MeV)	10 CFR 20 Fluence-to-Dose Equivalent Conversion Coefficient, h(E) (mrem/h)/(n/cm^2*sec)
2.5×10^{-8}	1.0204×10^{-6}
1.0×10^{-7}	1.0204×10^{-6}
1.0×10^{-6}	1.2346×10^{-6}
1.0×10^{-5}	1.2346×10^{-6}
1.0×10^{-4}	1.1905×10^{-6}
1.0×10^{-3}	1.0204×10^{-6}
1.0×10^{-2}	9.9010×10^{-7}
1.0×10^{-1}	5.8824×10^{-5}
5.0×10^{-1}	2.5641×10^{-5}
1.0	3.7037×10^{-5}
2.5	3.4483×10^{-5}
5.0	4.3478×10^{-5}
7.0	4.1667×10^{-5}
10.0	4.1667×10^{-5}
14.0	5.8824×10^{-5}
20.0	6.25×10^{-5}
40.0	7.1429×10^{-5}
60.0	6.25×10^{-5}
100.0	5.0×10^{-5}
200.0	5.2632×10^{-5}
300.0	6.25×10^{-5}

Table 2.1. Fluence per unit dose equivalent (h(E)) for neutrons.[58]

2.5 Phantoms

For the purposes of radiation protection, it is necessary to devise a "phantom" to mimic the properties of human tissue in a radiation field. Using a 15-cm radius sphere composed of a tissue equivalent material has the following advantages:

(1) It is relatively uncomplicated.
(2) The widely accepted specifications of its composition (tissue) allow ready comparison with calculations and measurements at other laboratories.
(3) It has an isotropic response to radiation.
(4) It is a reasonable phantom for calibration purposes (e.g. for personal dosimeters worn on the human abdomen).

While such a sphere can never be used to determine organ dose equivalents or the effective dose equivalent, it is very effective for purposes of radiation protection, and can be used to characterize the potential irradiation of an individual in terms of a single whole-body dose equivalent quantity.

In the simulations that are going to be performed for NPTC, a 15 cm radius sphere, composed of A-150 plastic, has been chosen. A 15-cm radius sphere also has the advantages of satisfying the size requirements necessary for use of the fluence-to-dose equivalent conversion coefficients described in Section 2.3. A-150 plastic has a mass composition of 77.55% carbon, 10.13% hydrogen, 5.23% oxygen, 3.51% nitrogen, 1.84% calcium, and 1.74% fluorine, which has been found to approximate the neutronic properties of human tissue very accurately.[36] The compositions used in the computer simulation are summarized in the Appendix.

2.6 Summary

In this section the basic mechanisms of neutron production from the operation of a proton accelerator were explained. The complexity of the neutron fields and the resulting effects on the neutron dose equivalent characteristics were also examined, and a simple

phantom was chosen to realistically simulate exposures to workers and member of the general public.

SECTION 3 - SHIELDING SPECIFICATIONS

3.1 Shielding Design Goals

The goal of proton therapy accelerator shielding designs is to attenuate the radiation produced in the accelerator and its associated equipment, of which neutrons are the dominant shielding concern, in order to protect patients, staff, and members of the general public. An efficient shielding design should minimize the cost without compromising the utility of the particle accelerator for its designed purposes. This is achieved in three stages:

(1) Determination of the neutron source terms (See **2.1, 3.2.2**)
(2) Specification of the acceptable dose equivalent levels outside the shielding (See **3.2.3**)
(3) Design of a shield with adequate attenuation to achieve the acceptable dose equivalent limits, with sufficient flexibility to permit efficient accelerator operation, with readily available materials and at optimum cost.

In the case of the Northeast Proton Therapy Center, stages 1 and 3 are complicated by the complex arrangement of proton beam transport equipment. At any point in the beam transport, stray protons can interact with the bending and focussing magnets, which may result in neutron production. Neutron production will also arise from protons interacting with the accelerator structure itself, the graphite energy degrader wheel of the energy selection system, and the various beam delivery systems. The energy of the proton beam, direction of incidence, and the beam stop locations and materials also influence the neutron source term. The arrangement and design of the some of the shielding barriers is complicated by the space and utility restraints, e.g., maze geometries to allow access to the cyclotron vault and treatment rooms.

3.2.1 The MGH NPTC Cyclotron and Beam Delivery Components

The NPTC cyclotron was designed by Ion Beams Applications (IBA) for the production of a proton beam suitable for clinical use.[26] The equipment setup is shown in Figure 3.1, showing the relative locations of the cyclotron, the energy selection system, the beam line, and the treatment rooms. Its major characteristics are:

(1) **Energy** - The NPTC cyclotron is a zero-gradient synchrotron, injected from a radiofrequency quadrupole at 2 MeV, fixed energy of 235 MeV. Nearly continuous energy selection is available by degrading the proton energy in a graphite absorber wheel with variable thicknesses. Monochromaticity of proton energy is provided by analyzing magnets and slits. This allows for a range of proton energies from 70 to 235 MeV.

(2) **Current** - Clinical currents usually run in the region of 10 nA, corresponding to approximately $6x10^{10}$ protons/s. The maximum beam current is 1.5 mA, but has been hardware limited to 300 nA for patient safety. This current is approximately equal to $2x10^{12}$ protons/s.

(3) **Beam Transport and Directionality** - The beam can be directed into either of two gantry treatment rooms, an experimental bay, an eye-treatment station, or a large-field treatment platform. The beam can only be directed to one of these stations at a time. The gantries rotate through 360 degrees and allow the beam to be pointed in any direction in a vertical plane.

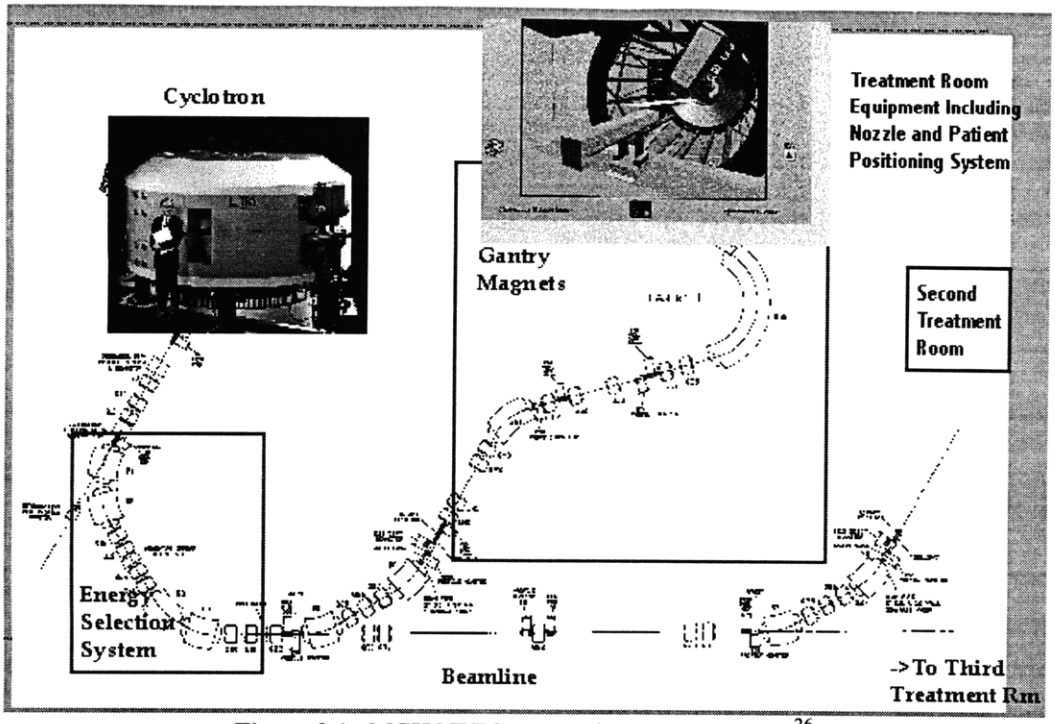

Figure 3.1. MGH NPTC proton therapy equipment.[26]

3.2.2 Determination of the Source Terms

Proton interactions with materials in the beamline can occur at any time during operation. Neutron production may arise from any of these interactions. The materials in the beamline that were intended to stop either all or some fraction of the proton beam at some time are termed 'beam stops,' e.g., a copper Faraday cup for measuring proton beam current or the patient being treated. The beam loss scenarios described in the following sections (3.2.2.1 and 3.2.2.2) were estimated by the NPTC Radiation Safety Committee and were used by Larson et al. for their shielding design work.[28,37]

3.2.2.1 Operational Beam Loss

There are many locations in the accelerator, proton energy selection system, and beam delivery equipment where protons can interact and produce neutrons. The shielding design by Larson et al.[37] assumes the three sets of copper beam stops recommended by the NPTC Safety Committee.[28] There will also be a degree of beam

loss within the energy degrader wheel, including energy loss through coulombic interactions and multiple coulomb scattering and current loss through (p,xn) reactions (see Section 2.2). However, the neutron source terms from the copper beamstops will tend to dominate as neutron production in high-Z materials (such as copper) is greater than that in low-Z materials (such as the carbon in the graphite beam stop). Directing the proton beam into beam stops is sometimes necessary for diagnostic purposes. Following are the design specifications from the NPTC Radiation Safety Committee, which were formulated to prevent accelerator personnel from exceeding the capabilities of the neutron shielding:[28]

(1) The first beam stop is located at the degrader wheel, and the proton beam will be stopped there for no more than 0.5 h/day. Average current incident on the beamstop should not exceed 50 nA, and the shielding should be adequate to allow a 300 nA beam to be stopped at the degrader for up to 15 min/week.

(2) The second beam stop is located downstream of the beam profile monitor after the collimator. The beam will be stopped at this point for no more than 5 h/week, and the current should not exceed 10 nA.

(3) The third beamstop is the set of beamstops located at the entrances to the gantry rooms. The beam stopped at these locations should not exceed $4x10^{12}$ protons at 235 MeV in any hour and shall not exceed $5x10^{12}$ protons at 235 MeV per 40 h of operation.

3.2.2.2 Clinical Beam Loss

During clinical operation in the gantry treatment rooms, the large fraction of the total beam current will be delivered to the patient. Averaged over 40 hours of operation, these proton losses are assumed to be $1.34x10^{12}$ protons/h at 150 MeV, $3.32x10^{12}$ protons/h at 200 MeV, and $1.87x10^{12}$ protons/h at 235 MeV.[28]

3.2.2.3 Occupancy Factors

The ambient dose equivalent levels can be modified by "occupancy factors" that take into account the amount of time the irradiated areas are occupied by workers or members of the general public. The following are the recommendations of the NPTC Radiation Safety Committee:[28]

(1) All normal contiguous interior work areas, including patient waiting areas, shall be assigned an occupancy factor of 1.
(2) Areas such as emergency access or repair areas may be assigned an occupancy factor of ¼.
(3) Exterior areas that are used ony for pedestrian or vehicular traffic may be assigned a factor of 1/16.
(4) The barrier shielding the parking lot should be assigned a factor of ¼ provided that there is no attendant on duty. If the lot is attended, that factor must be 1.
(5) Areas can be interlocked to exclude occupancy during periods of machine operation. These areas can be assigned an occupancy factor of 0.

3.2.3 Dose Limits

The following are the dose limits used in the design of the NPTC:

(1) The maximum weekly occupational dose shall not exceed 10 mrem.
(2) The maximum weekly dose to a member of the public shall not exceed 2 mrem, subject to occupancy factors.
(3) The maximum weekly occupational dose to the extremities shall not exceed 1 rem.
(4) The dose in unrestricted areas shall not exceed 2 mrem in any single hour, given the worst case radiation level produced.
(5) The maximum yearly total effective dose equivalent shall not exceed 100 mrem.

The MGH safety committee specified that the radiation protection program at NPTC is to satisfy the regulations of the Commonwealth of Massachusetts, the Nuclear Regulatory Commission, the Environmental Protection Agency, and shall satisfy the additional requirements set forth by MGH in reference [37]. While state regulations have precedence over federal in terms of local radiation protection dose limits, Massachusetts became an agreement state in 1997, in effect making the federal regulations and the

regulations of the Commonwealth inclusive.[58] The dose limits above represent the most restrictive combination of this set of regulations.

3.3 Neutron Attenuation

Neutrons are stopped in shielding through a two-step process. The first step is moderation, in which the neutron energy is reduced through scattering reactions. The second step is absorption, where the neutron is taken up by a nucleus and removed entirely. The neutrons produced by the interaction of the proton beam with materials in the beam path propagate from the beam stop and into the shielding walls. Those neutrons that escape from the shielding are the neutrons that contribute to the dose equivalent that the workers and general public may receive. The degree to which the initial intensity of the neutron field is reduced is termed the attenuation of the neutron field. Neutrons lose energy and are absorbed as they propagate through the shielding structure through inelastic and elastic collisions with nuclei in the wall. Above 10 MeV, inelastic collisions and non-elastic reactions tend to dominate the energy loss mechanism, while for neutron energies ranging from a few eV to a few MeV, elastic collisions tend to dominate. In the thermal energy range ($E_n < .025$ eV) neutrons are removed through the process of neutron capture.[31]

The cross section for inelastic collisions of high energy neutrons with nuclei increases with the atomic number of the nuclei. For energies up to approximately 20 MeV, the inelastic cross section (σ_i) varies roughly as the quasi-physical cross section of the nucleus, $\sigma_i \sim A^{2/3}$. As the neutron energy increases, this cross section tends to decrease. This is because the nucleus, from the standpoint of the incident neutron, looks less and less like a solid aggregate and more like a collection of individual nucleons. The nucleus becomes "transparent," allowing high energy neutrons a greater probability of passing through without interaction. This cross-sectional falloff is more rapid for light nuclei such as silicon than for heavier nuclei such as iron. On the other hand, low-Z materials such as hydrogen will attenuate neutrons very rapidly because the neutrons tend

to lose more of their energy on average in a single collision. The average logarithmic energy loss ξ in a single scattering is:

$$\xi = 1 + \frac{\alpha}{1-\alpha} \ln \alpha \qquad (3.1)$$

where

$$\alpha = \left(\frac{A-1}{A+1}\right)^2 \qquad (3.2)$$

and A is the mass of the recoil nucleus. Thus, a fast neutron field is most readily moderated by a combination of relatively high-Z materials and materials with large hydrogen content.[31] Once these neutrons have been moderated to thermal energies, they can be absorbed through neutron capture in the nuclei that make up the shielding.

Concrete provides this combination relatively inexpensively, and due to its mechanical characteristics it has the added benefit of being a viable structural material. While shields consisting of layers of iron and lead or mixtures of concrete and polyethylene may provide more attenuation of neutrons per unit thickness than concrete shielding alone, they have significantly higher material and fabrication costs, and tend to be mechanically unsound without additional support structures.[7]

Using the Moyer model for dose equivalent (Equation 3.3) as a function of beam current **I**, the beam loss scenario described in Section 3.2.2, and the maximum allowed dose equivalent in the environments adjacent to the accelerator and treatment rooms described in Section 3.2.3, the following expression (Equation 3.4) can be derived for the estimation of the shield thickness $x(\theta)$ in meters with θ being the secondary particle (neutrons in this case) polar angle with respect to the proton beam direction:

$$H_{outside} = \frac{H(\theta)_{inside} \bullet I \bullet p_{loss}}{r^2} e^{x(\theta)m(\theta)} \qquad (3.3)$$

$$x(\theta) = \frac{1}{m(\theta)} \cdot \ln\left(\frac{H(\theta) \bullet I \bullet p_{loss}}{H_{max} \bullet r^2}\right) \qquad (3.4)$$

where $\mu(\theta)$ is the mean attenuation coefficient of neutrons in the shield material in the direction θ with units m^{-1} (see Table 3.3), H_{max} is the maximum allowed dose equivalent rate behind the shield (2 mrem/h in this case), r is the distance between the source and the point of interest in m, $H(\theta)$ is the source term in mrem/h along the direction θ, I is the proton current in ions per second, and p_{loss} is the beam loss fraction.[1]

Neutron Energy (MeV)	$\mu(\theta)$ (m^{-1})	Neutron Energy (MeV)	$\mu(\theta)$ (m^{-1})
5	8.22	65	3.62
10	8.22	70	3.45
15	7.92	75	3.31
20	7.38	80	3.19
25	6.96	85	3.07
30	6.45	90	2.96
35	5.94	95	2.87
40	5.49	100	2.79
45	4.92	150	2.26
50	4.49	200	2.09
55	4.13	250	2.06
60	3.84		

Table 3.3. Attenuation factors used for Bechtel shielding concrete.[7]

3.4 Summary

In this section, the requirements for neutron shielding were discussed. The characteristics of the Northeast Proton Therapy Center have been described, and the general specifications for the neutron shielding in terms of the neutron sources, dose equivalent limits, and factors that influence the choice of shielding material were explained. In Section 4, a means by which several of these factors can be integrated into a complex mathematical model will be described.

SECTION 4 - COMPUTATIONAL SOLUTIONS

Much of the previous work in neutron shielding has utilized analytical models,[1,2,9,28,30] based on approximations that may introduce significant uncertainties, including the restriction to a one-dimensional geometry, the assumption that all secondary particle production is in the forward direction, and the assumption that particle production is represented by rather simple analytic expressions. These approximations introduce uncertainty into the predicted shielding barrier thicknesses.

4.1 Monte Carlo Approach

Monte Carlo methods for solving difficult stochastic problems have been used in some form or another for decades, following the formulation of Monte Carlo theory by von Neumann in 1947.[33] In using a Monte Carlo approach to the solution of the radiation transport equations, the problem is formulated as a succession of individual processes rather than in terms of macroscopic quantities. The particles to be simulated, usually referred to as a particle history or as a 'cascade,' are transported by constructing a mathematical 'experiment.' Particle histories comprise the trajectory of the particle, including interaction events, e.g., elastic or Coulomb scattering events, or inelastic nuclear events. A history terminates when the particle leaves the domain of the geometric model, when its energy drops below a certain threshold level, or when it is absorbed. The interaction processes and particle productions are selected at random from a probability distribution which is either expressed in the form of theoretical or empirical equations or represented by experimental data in tabular form.[11,41] Figure 4.1 illustrates the random history of a neutron incident on a slab of material that can undergo an evaporative and intranuclear cascade process. In this example, the incident neutron enters and undergoes a scattering event at point 1. The scattered neutron travels to point 2, where it undergoes an intranuclear cascade reaction, resulting in the scattering of the initial neutron and the ejection of a second neutron. The first neutron escapes at point 4a. The second neutron travels to point 3, where it undergoes a capture process, resulting in

evaporation of two neutrons. The first escapes at point 4b, the second is captured at point 5.

Event Probability	Event Type
0.20	(1) Neutron Scatter
0.30	(2) Intranuclear Cascade
0.10	(3) Neutron Absorption with Evaporation
0.35	(4) Neutron Leakage
0.05	(5) Neutron Capture

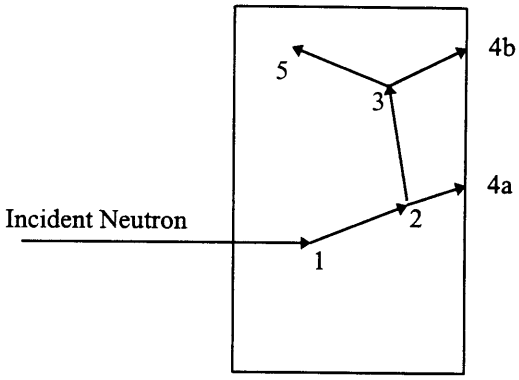

Figure 4.1. Monte Carlo simulation of a neutron incident on a slab of material.

At any point in the cascade simulation, any required macroscopic physical quantity, such as particle fluence, energy fluence, absorbed dose, and/or density of inelastic interactions may be 'scored'. To 'score' these quantities means that the individual contribution to the required physical quantity from the particle being followed may be computed and stored. When a statistically significant number of particles (i.e., within the desired statistical significance for the specified tally regions) have been scored, the calculated values of the designated physical quantities may be evaluated to the required statistical accuracy (usually < 5%).

In principle, none of the limitations of the analytical solutions listed above apply to the Monte Carlo method. In particular, any three-dimensional geometrical configuration containing many different media may be considered. The main disadvantage of the Monte Carlo method is that the simulation of realistic shielding problems with good statistical accuracy requires considerable computer resources.

4.2 Transport Codes

4.2.1 Historical Summary of LAHET and its Precursors

The first fully developed multi-purpose Monte Carlo charged particle transport code to become generally available was the High Energy Transport Code (HETC).[55] HETC allows for the simulated transport of nucleons, pions, and muons, and was originally developed by the Neutron Physics Group at Oak Ridge National Laboratory. [46] It has for many years been a benchmark for heavy charged particle cascade codes used in radiation physics and radiation protection.

The main feature of HETC is its incorporation of an intranuclear cascade plus evaporation model to determine the products (along with their energies, angular distributions, and multiplicities) from non-elastic collisions. The earliest version of the code was developed by Coleman[15] and was then known as the NMTC code. It was limited to the calculation of cascades induced by protons of energies less than 3 GeV. The kinetic properties of the nuclear collision products were obtained by employing the intranuclear cascade code developed by Bertini.[4,5] Below 25 MeV, charged particle interactions were neglected and neutrons were transported using the O5R Monte Carlo program.[27] The code has undergone many revisions since then, with Bertini's earlier intranuclear cascade code replaced by his newer MECC-7 code[6] and the evaporation portion replaced by Guthrie's EVAP-4 code. [18]

As an alternative to the Bertini intranuclear cascade model, the Los Alamos High Energy Transport code (LAHET) contains the intranuclear cascade routines from the ISABEL code. The ISABEL intranuclear cascade model is an extension developed by Yariv and Fraenkel[62] of the VEGAS code.[12] It has the capability of treating nucleus-nucleus interactions as well as particle-nucleus interactions. It allows for interactions between particles, both of which are excited above the Fermi sea.[63] The nuclear density is represented by up to 16 density steps, rather than three as in the Bertini intranuclear cascade model. It also allows antiproton annihilation,[13] with emission of kaons and pions. As presently implemented in LAHET, only projectiles with $A \leq 4$ are allowed, and antiproton annihilation is not presently allowed in particle transport problems.

Subsequent de-excitation of the residual nucleus may optionally employ a multi-stage pre-equilibrium exciton model.[42] The multi-stage pre-equilibrium model is invoked at the completion of each intranuclear cascade, with an initial particle-hole configuration and excitation energy determined by the outcome of the cascade. At each stage of the multi-stage pre-equilibrium model, the excited nucleus may emit a neutron, proton, deuteron, triton, ^{3}He, or alpha particle or the nuclear configuration may evolve toward an equilibrium exciton number by increasing the exciton number by one particle-hole pair. When the multi-stage pre-equilibrium model reaches the equilibrium exciton number, it terminates. The evaporation model or Fermi breakup model is then applied to the residual nucleus with the remaining excitation energy.[44]

In LAHET, the Fermi breakup model[8] has replaced the evaporation model for the disintegration of light nuclei. It treats the de-excitation process as a sequence of simultaneous breakups of the excited nucleus into two or more products, each of which may be a stable or unstable nucleus or a nucleon. Any unstable product nucleus is subject to subsequent breakup. The probability for a given breakup channel is primarily determined from the available phase space, with probabilities for two-body channels modified by Coulomb barrier, angular momentum, and isospin factors. The model is applied only for residual nuclei with $A \leq 17$, replacing the evaporation model for these nuclei. In the LAHET implementation, only two- or three-body breakup channels are considered, which is an abbreviated form of a more extensive implementation of the Fermi breakup model.[8]

LAHET differs from HETC in the use of cutoff energies for particles escaping from the nucleus during the intranuclear cascade. For either intranuclear cascade model, the neutron cutoff energy is uniformly distributed between zero and twice the mean binding energy. The Coulomb barrier is randomly distributed in a form simulating a Coulomb barrier transmission probability; the maximum of the Coulomb barrier and a neutron cutoff is then used as the proton cutoff. The sampling for the cutoff energies is

performed once for each projectile-target interaction; the barriers thus defined are then applied to every particle emission in the resulting cascade. This procedure has the effect of preventing a discontinuity in the particle emission spectrum while preserving the mean particle emission rates. [45]

Another small addition to the intranuclear cascade procedure that is particularly important to the neutron shielding calculations to be performed in this work is applied to (p,n) and (n,p) intranuclear cascade reactions only. In this case, the outgoing particle energy is corrected by the binding energy difference in the entrance and exit channels. The modification greatly improves the realism in the high energy emission spectrum and significantly improves the overall energy balance in the intranuclear cascade reaction. [45]

4.2.2 LAHET Code System Organization

The LAHET Code System (LCS) is a set of codes based on LAHET for the transport and interactions of nucleons, pions, muons, light ions, and antinucleons in a complex geometry.[43] It has been extensively benchmarked, with calculations compared against experimental results for energies up to 256 MeV, which more than covers the energy ranges of clinical interest at NPTC. [44,45] For the purposes of this work, an updated version of LAHET[46] has been used, along with the addition of a post-processing code (PROCESS). The linking is shown below in Figure 4.2.

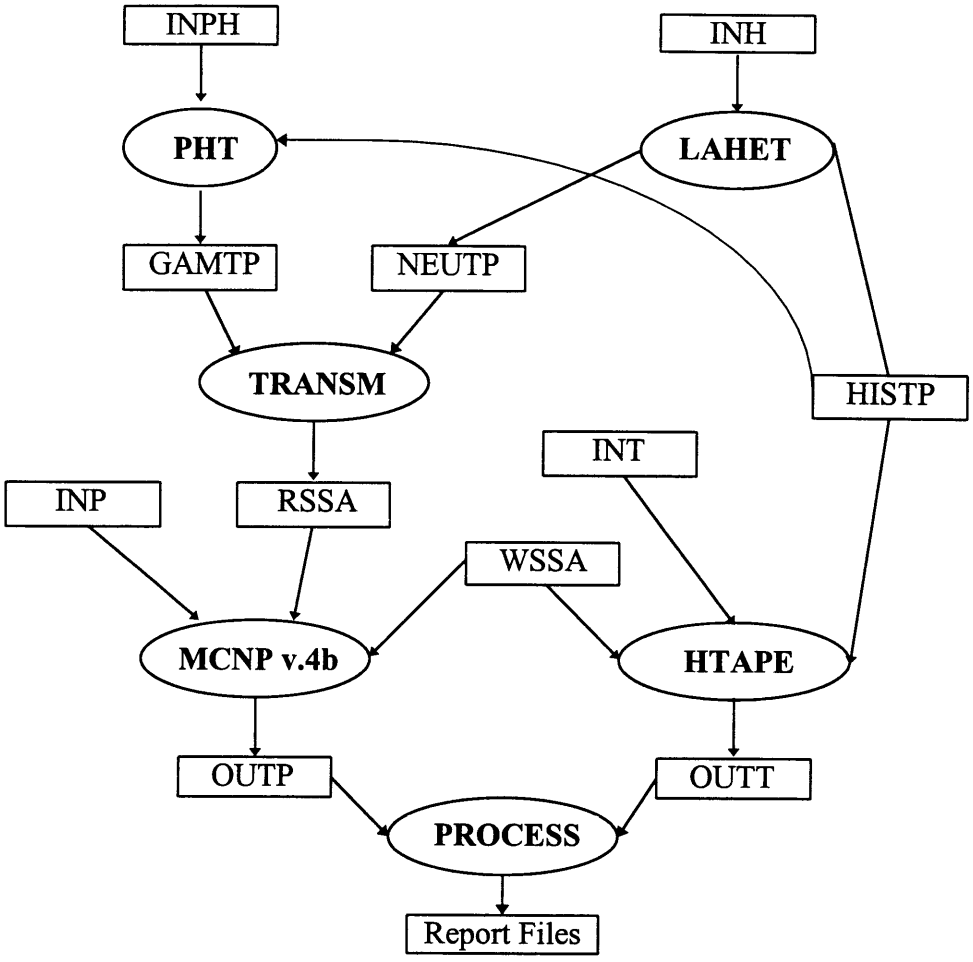

Figure 4.2. Program linkage used by the LCS for the purposes of this work.

Particle tracking uses the combinatorial geometry model from the MCNP code.[11] LAHET shares the geometry description and input of MCNP, except for some of the finer points, such as lattices and repeated structures, which are absent in LAHET. Charged particle transport uses continuous slowing-down interaction models that optionally incorporate range-straggling and multiple scattering adapted to MCNP geometry. In addition, a LAHET history file (HISTP) may be used to generate a surface source for a subsequent LAHET calculation.[45]

In LAHET, neutrons with energies below 20 MeV are written to a source file for transport with MCNP version 4b. MCNP v.4b accepts external neutron/photon sources

created by LAHET through the use of the TRANSM code.[46] TRANSM accepts the low-energy surface crossing records (NEUTP for neutrons and GAMTP for photons) and writes them to a surface-source read file (RSSA). Neutron transport from 20 MeV to thermal energies and all photon/electron transport is then performed by MCNP v.4b, using this source file. It may also be used for coupled neutron/photon/proton multigroup calculations with a limited number of isotopes at energies below 100 MeV. The output from MCNP v.4b is written to a surface-source write file (WSSA) across a set of user-defined surfaces. MCNP v.4b can also perform edits on the surface crossing records, including tallies of surface current and surface flux, a track length estimate of fluence and energy deposition, and the deposition of charge. This information is then written to an MCNP v.4b output file (OUTP).

Editing of the LAHET history file is accomplished with HTAPE, a general-purpose particle history editor. Edits include surface current, surface flux, neutron volume flux, particle production spectra, energy deposition and balance, distribution of residual nuclei and excitation, gas production, and pulse shape characteristics.[43] HTAPE combines the output from the high-energy (above 20 MeV) neutron surface-crossing histories (HISTP) with the MCNP v.4b output (WSSA) to evaluate the above quantities. Unfortunately, due to the fact that HTAPE can only read in surface crossing records from the WSSA file, the only edits that it can perform that are applicable to the determination of neutron dose equivalent are the surface current and surface flux edits. In order to perform tallies such as energy deposition or track length estimate of flux, a separate program (PROCESS) must be invoked that can read the tallied information from the MCNP v.4b OUTP file and included in the higher energy neutron edits performed by the HTAPE program. This user supplied program will be discussed in greater detail in Section 5.5.

SECTION 5 - THE MONTE CARLO STUDY

5.1 Modeling Considerations

For studying the neutron shielding problem, the system of codes (LCS) described in section 4.2.2 has been implemented. A Hewlett-Packard workstation running HP UNIX v.10.20 was configured as the platform on which to run the various programs. The considerations that must be dealt with in developing a Monte Carlo model for this shielding situation are 1) the development of a geometry that realistically reflects the shielding design used in the proton therapy facility, 2) the determination of the neutron source terms, 3) the characterization of the materials present in the problem, 4) the development of methods to handle the massive influx of data generated in the course of the LAHET calculation and subsequent editing, and 5) determining how best to interpret the data generated.

5.2 Shielding Geometry

The geometry was modeled using the as-built shielding designs provided by Bechtel Corporation (Figure 5.1).[7] These designs accurately portray the bulk shielding of the Northeast Proton Therapy Center, but omit some modifications made to the shielding during construction, such as the inclusion of ducts and other conduits through the shielding wall.

The NPTC shielding geometry model, comprising over 200 contiguous cells composed of approximately 150 unique surfaces, is shown below in Figures 5.2 and 5.3 with the aid of the 2-dimensional MCPLOT function provided with the MCNP4b package[11] and the 3-dimensional SABRINA visualization package,[59] as shown in Figure 5.4. Software detectors (tally regions) have been distributed throughout the NPTC facility, including one at each of the calculation locations chosen by Larson et al.[28] in

their shielding study. The locations of the tally regions on the treatment level are depicted as small spheres in Figure 5.2.

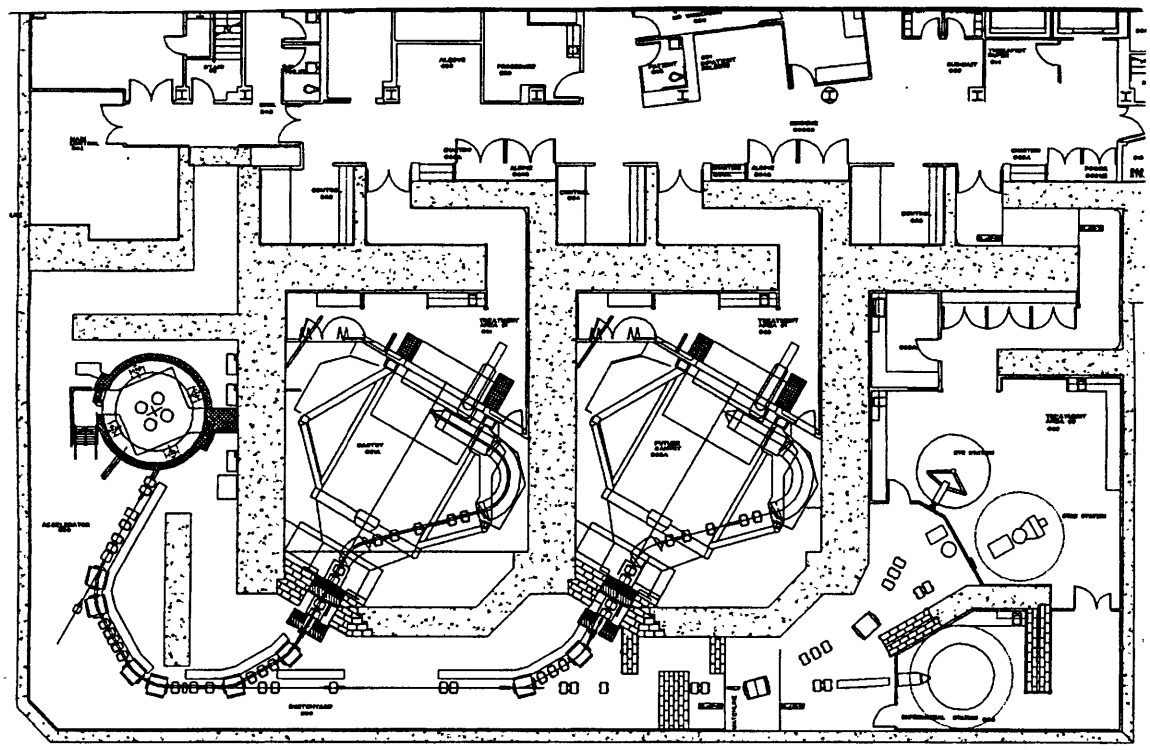

Figure 5.1. As-built drawing of the treatment level shielding.[7]

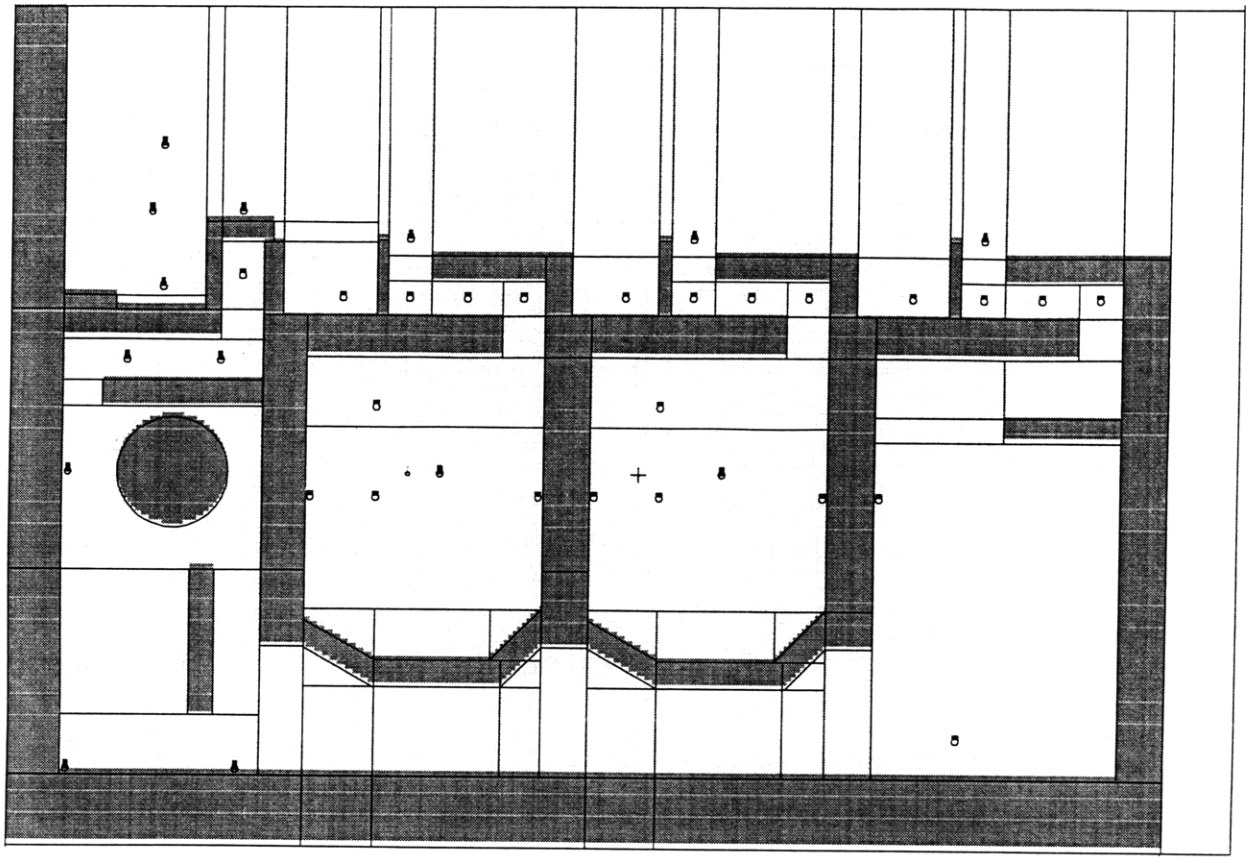

Figure 5.2. 2-dimensional plan view of NPTC treatment level. The software detectors are shown as small circles.

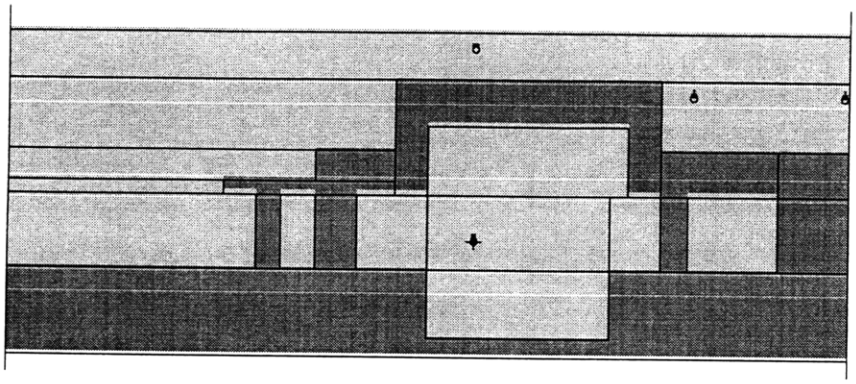

Figure 5.3. 2-dimensional side view of NPTC, cut through Gantry Bay 1. The software detectors are shown as small circles.

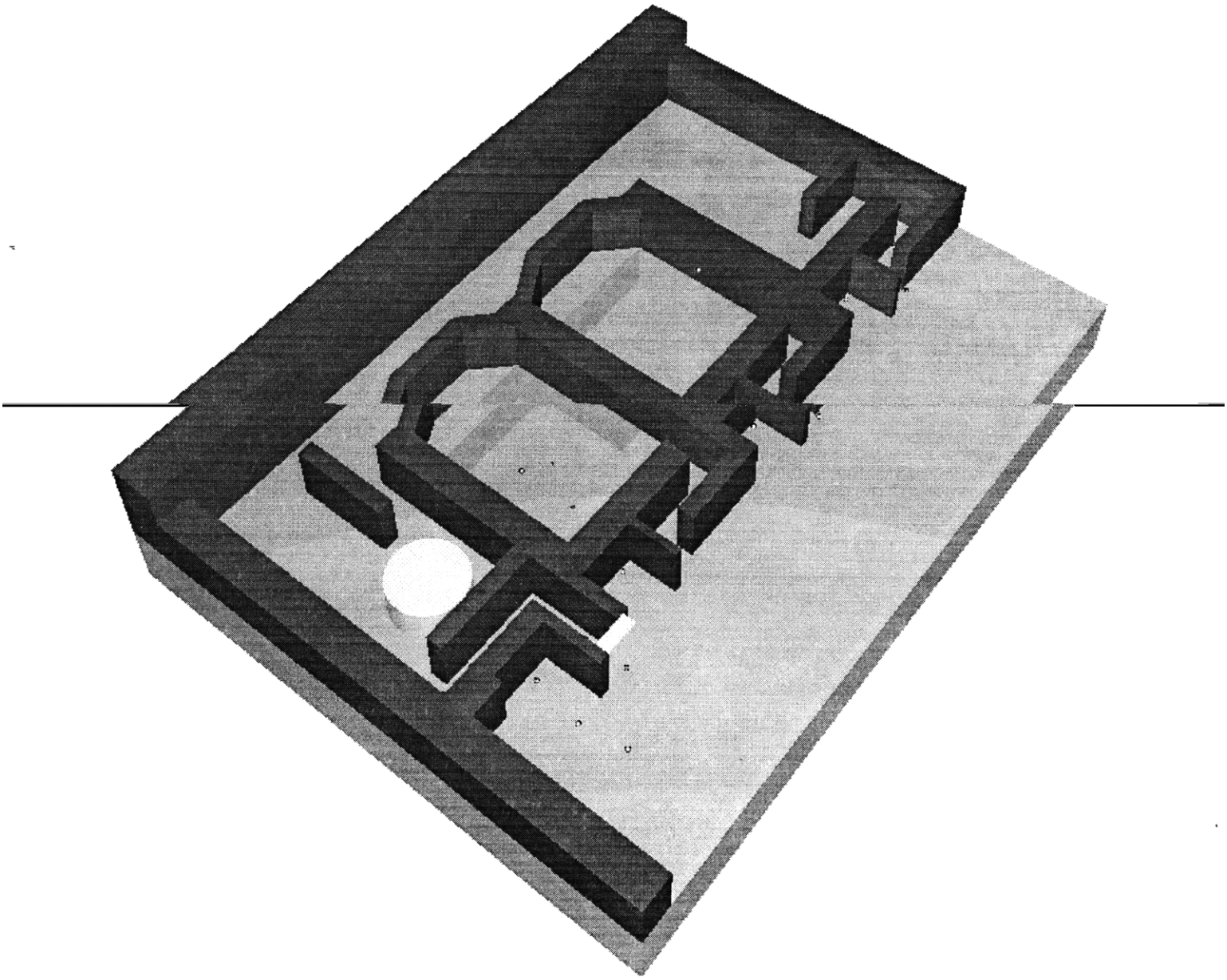

Figure 5.4. 3-dimensional view of NPTC bulk shielding.

5.3 Source Terms

Our preliminary shielding simulations include only one neutron source, which comprises an isotropic proton source located within a 10-cm sphere of copper. The geometry of an isotropic source within the beamstop was chosen because the version LAHET available for this study does not currently allow for a parallel beam source with arbitrary initial direction. Moreover, unlike MCNP v.4b, LAHET does not allow for transformation of the geometry coordinates with a transformation card.[11,43] While the use of an isotropic source is not entirely realistic, it provides an adequate source for testing

and code development work. Modifications are being made to the LCS to allow for full directional biasing of the source. The spectral fluences for neutron sources comprising a 10-cm copper sphere (beam stop) and a 15-cm tissue equivalent sphere (patient) were then computed for incident proton energies of 150, 200, and 235 MeV, the clinical loss energies described in Section 3.2.2.2. The emission spectra at the surfaces of these sources are shown in Figures 5.5 through 5.10 below.

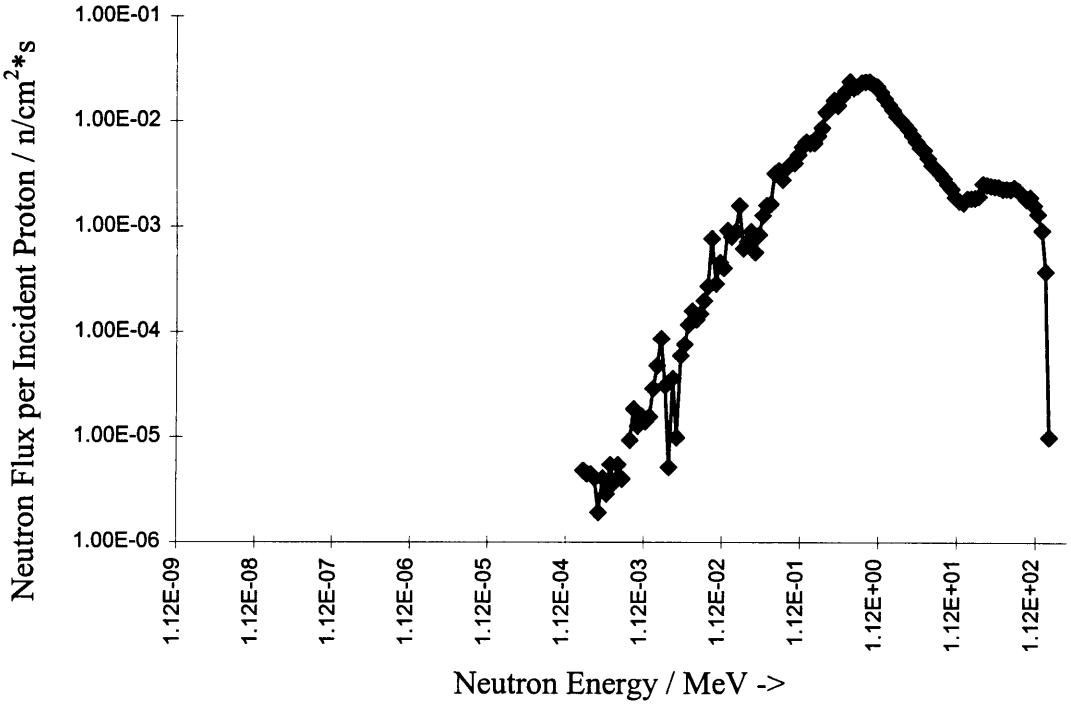

Figure 5.5. Neutron spectral fluence for neutrons produced by a 150 MeV isotropic proton source in a 10 cm sphere of copper.

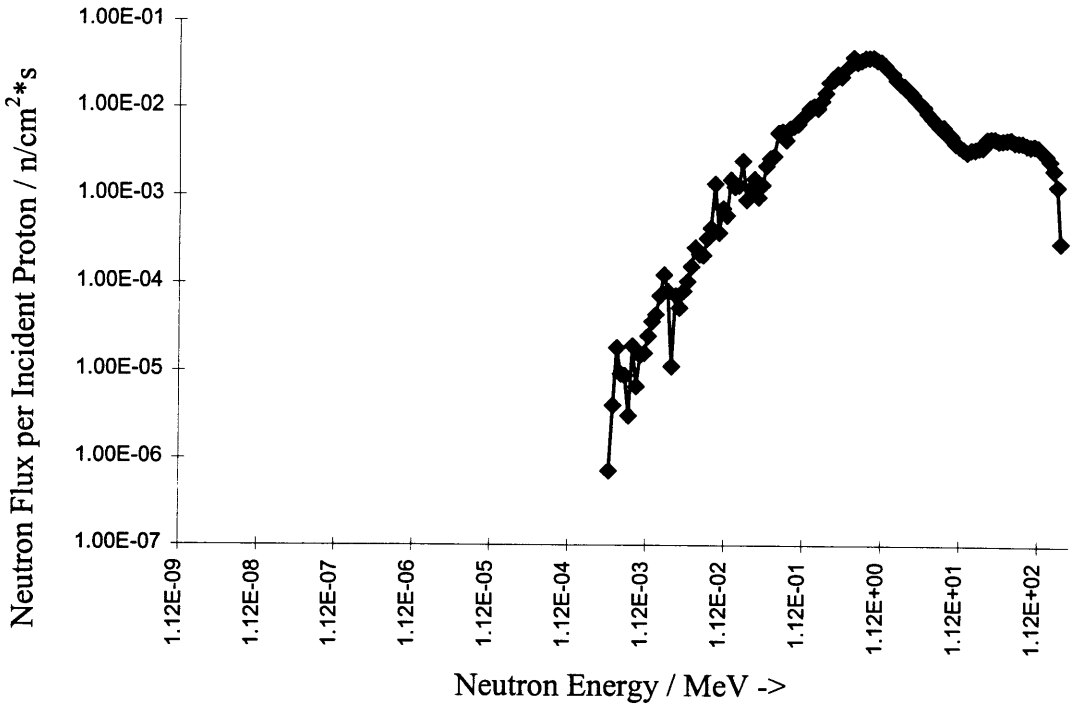

Figure 5.6. Neutron spectral fluence for neutrons produced by a 200 MeV isotropic proton source in a 10 cm sphere of copper.

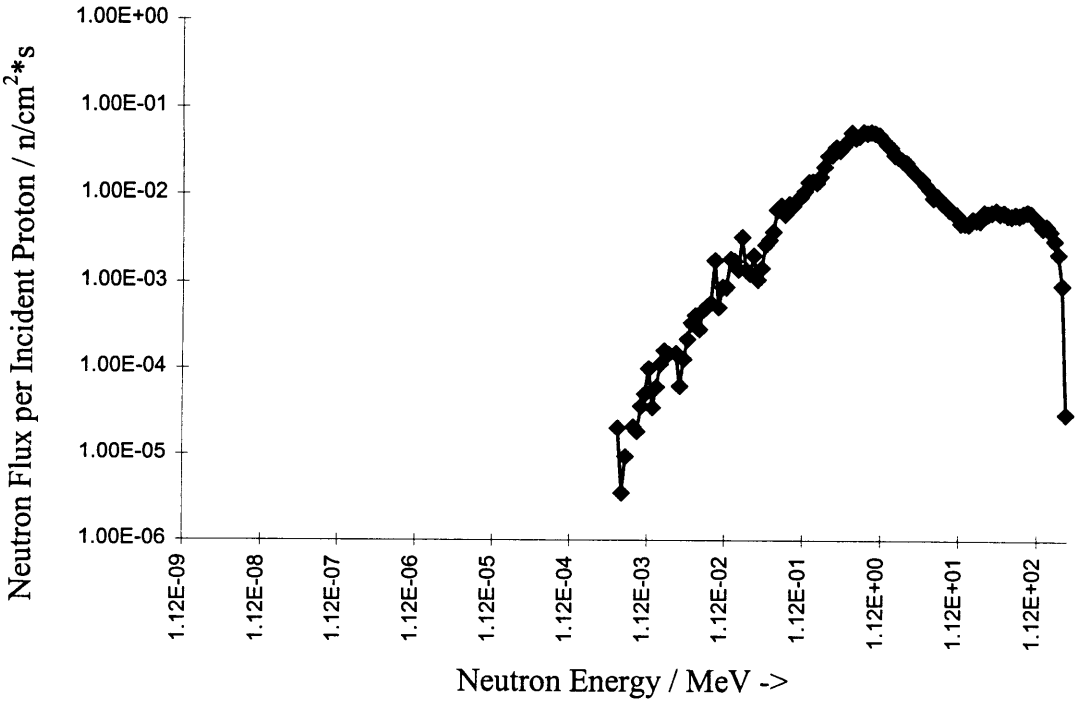

Figure 5.7. Neutron spectral fluence for neutrons produced by a 235 MeV isotropic proton source in a 10 cm sphere of copper.

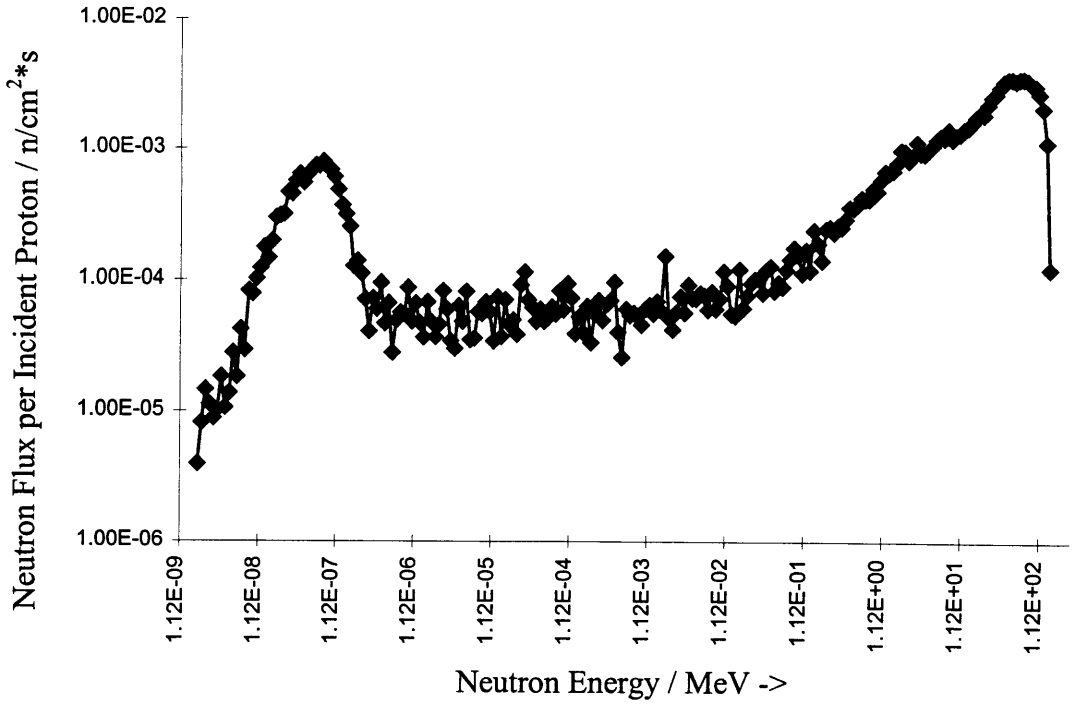

Figure 5.8. Neutron spectral fluence for neutrons produced by a 150 MeV isotropic proton source in a 15 cm sphere of A-150 tissue equivalent plastic.

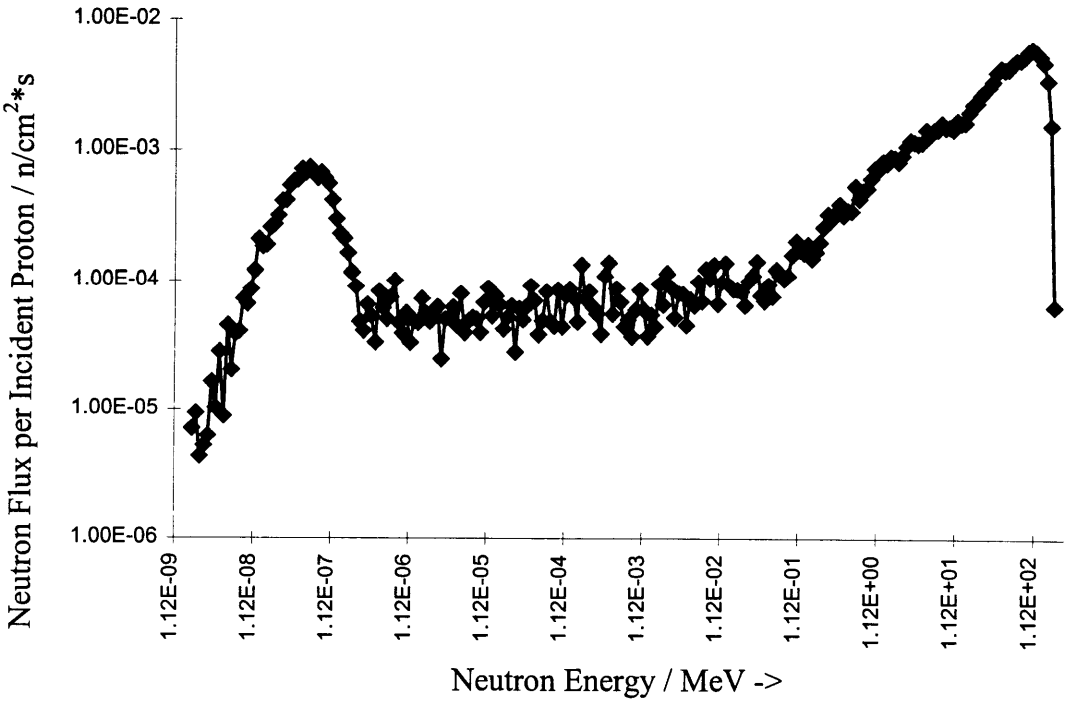

Figure 5.9. Neutron spectral fluence for neutrons produced by a 200 MeV isotropic proton source in a 15 cm sphere of A-150 tissue equivalent plastic.

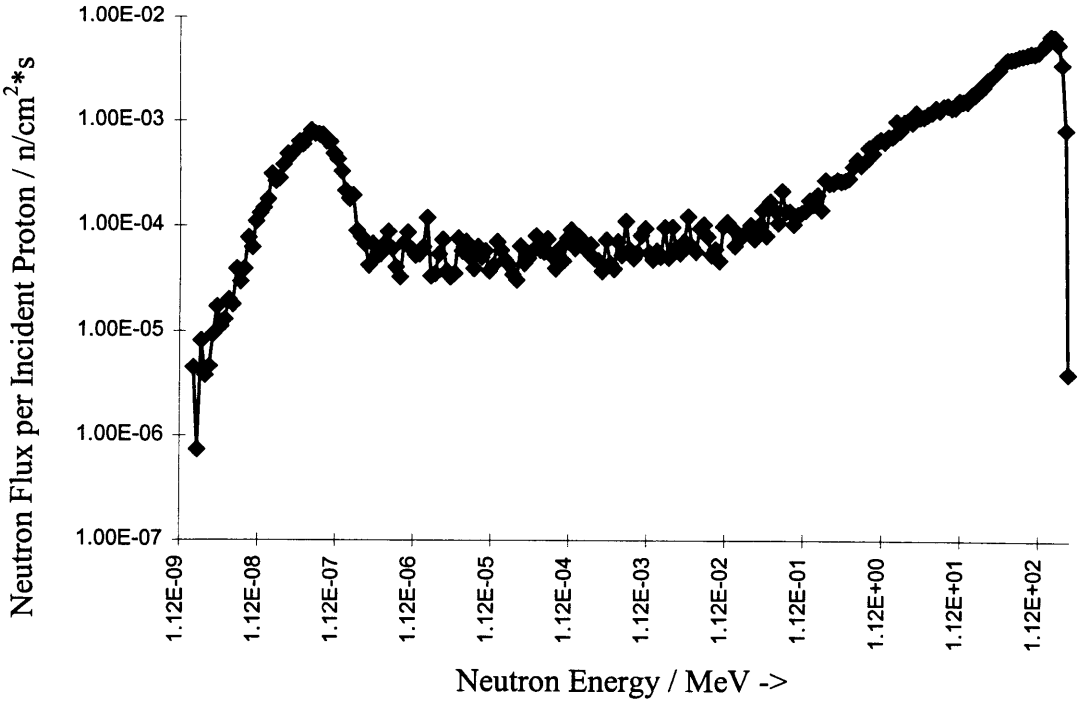

Figure 5.10. Neutron spectral fluence for neutrons produced by a 235 MeV isotropic proton source in a 15 cm sphere of A-150 tissue equivalent plastic.

This approximation of the source term provides a full energy range of neutrons to transport using LAHET and MCNP4b.

5.4 Shielding Material

The discussion of materials appropriate for the shielding of fast neutrons is covered in Section 3.3. The shielding concrete used by Bechtel is composed primarily of hydrogen, carbon, oxygen, magnesium, silicon, and calcium, presenting a wide variety of light nuclei for neutron moderation and heavier nuclei for neutron absorption. The proton and neutron elastic scattering cross-section data libraries available for LAHET are not complete for all elements. Therefore, for elements that do not have elastic cross-sections for use in LAHET, the proton and neutron elastic scattering cross-sections of heavier elements were substituted. For example, there is no elastic scattering cross-sectional information presently available for calcium or magnesium, two constituents of the NPTC shielding concrete, available in LAHET. To overcome this deficiency elements with

larger mass numbers, such as titanium and aluminum, can be used instead. This is actually conservative because elements with larger mass number A have lower moderating properties, an assertion that is supported in [64] and can also be quantitatively defended by means of the average logarithmic energy loss ξ in a single scattering, as described by equations 3.1 and 3.2 in Section 3.3. This works out to an ξ of 0.0492 for Ca, 0.0411 for Ti, 0.0811 for Mg, and 0.0723 for Al. The mass fractions and nuclear densities of NPTC shielding concrete and of air are included in the Appendix.

5.5 Data Processing and Analysis

Modeling this problem in the fullest possible detail is a formidable problem in terms of organization and data handling. The calculation the neutron dose equivalent values requires the combination of neutron source terms arising from approximately 63 discrete proton-induced neutron sources at several proton beam energies ranging from 70 to 235 MeV, with protons incident on several beam stop materials (e.g., graphite, tissue-equivalent plastic, copper, iron). The shielding performance from these sources is then to be calculated at roughly 50 locations to determine the average neutron dose equivalent and peak neutron dose equivalent rate. To minimize the time needed to model each of these possible sources individually and to handle the massive amounts of information generated, computer programs been written for the automated creation of LAHET input files and for post processing of the LAHET output files.[36]

A simulation with the LAHET code requires enormous amounts of disk space. This is because LAHET writes a detailed interaction history for each particle transported. For example, to simulate the transport of 100,000 protons through the geometry developed for the NPTC results in over 100 Mbytes of data. To run a simulation that is capable of attaining statistics acceptable for a scientific study would require the transport of tens or even hundreds of millions of particles. This would require terabytes of disk storage space, which is simply beyond our present day resources. To deal with this situation, a program that allows the user to combine the selected output data from a large

number of smaller runs into a single file has been written and is in the process of being tested.

The LAHET code does not predict the neutron dose equivalent values directly. Like MCNP, an edit program (HTAPE) reads in the surface crossing and interaction data from the history files and recovers the information pertinent to the type of tally being performed. Due to the edit limitations discussed in Section 4.2.2., HTAPE editing is limited to those edits that are derived from surface crossing records, such as neutron surface flux or surface current. The quantities provided by HTAPE are in neutron fluence (neutrons/cm^2) per incident neutron. This value can be multiplied by the ratio of the number of neutrons created in the simulation to the number of protons simulated to obtain the neutron spectral fluence per incident proton. Energy dependent fluence-to-dose equivalent conversion coefficients are available from the literature, and provide one way by which the predicted neutron spectral fluences can be converted into a neutron dose equivalent values.[20,35,58] (Figure 5.3, also Section 2.3) The post-processing code discussed in Section 5.5 is currently undergoing modification to allow the > 20 MeV edits performed by HTAPE to be merged with the < 20 MeV edits performed by MCNP, bypassing the surface crossing restriction entirely and allowing for the full range of tallies to be utilized.

Neutron Energy (MeV)	NCRP-38[35] Fluence-to-Dose Equivalent Conversion Factor (mrem/h)/(n/cm^2•s)	ICRP-21[20] Fluence-to-Dose Equivalent Conversion Factor (mrem/h)/(n/cm^2•s)
2.5E-08	3.67E-03	3.85E-03
1.0E-07	3.67E-03	4.17E-03
1.0E-06	4.46E-03	4.55E-03
1.0E-05	4.54E-03	4.35E-03
1.0E-04	4.18E-03	4.17E-03
1.0E-03	3.76E-03	3.70E-03
1.0E-02	3.56E-03	3.57E-03
1.0E-01	2.17E-02	2.08E-02
5.0E-01	9.26E-02	7.14E-02
1.0	1.32E-01	1.18E-01
2.0		1.43E-01
2.5	1.25E-01	
5.0	1.56E-01	1.47E-01
7.0	1.47E-01	
10.0	1.47E-01	1.47E-01
14.0	2.08E-01	
20.0	2.27E-01	1.54E-01
40.0		

Table 5.3. Neutron fluence-to-dose equivalent rate conversion coefficients.

5.6 Uncertainties

The major difficulty presented in the use of Monte Carlo methods in systems that comprise large geometries and a high degree of attenuation is that very few particles actually reach the points where tallies are being performed. This creates a high degree of uncertainty in the calculations unless a large number of particles can be run. The uncertainty is quantified in LAHET and MCNP by the relative error per starting particle history,

$$R = \frac{S_{\bar{x}}}{\bar{x}} \qquad (5.1)$$

where

$$S_{\bar{x}} = \sqrt{\frac{S^2}{N}}, \qquad \bar{x} = \frac{1}{N}\sum_{i=1}^{N} x_i \qquad (5.2,5.3)$$

and N is the total number of particle histories. However,

$$\overline{x^2} = \frac{1}{N}\sum_{i=1}^{N} x_i^{\,2} \text{ and } S = \sqrt{\overline{x^2} - (\bar{x})^2} \qquad (5.4,5.5)$$

combining,

$$R = \sqrt{\frac{\sum_{i=1}^{N} x_i^{\,2}}{\left(\sum_{i=1}^{N} x_i\right)^2} - \frac{1}{N}}. \qquad (5.6)$$

For a problem where nonzero scores occur very infrequently, such as in a large geometry, heavily attenuating problem,

$$\frac{1}{N} \ll \frac{\sum_{i=1}^{N} x_i^{\,2}}{\left(\sum_{i=1}^{N} x_i\right)^2} \qquad (5.7)$$

so let n_i = the number of nonzero scores per run that are equal to x, $n_i \ll N$, so

$$R_i \approx \left(\frac{n_i x^2}{n_i^{\,2} x^2}\right) = \frac{1}{\sqrt{n_i}} \qquad (5.8)$$

for $n_i \ll N$, where R_i is the relative uncertainty calculated per run.

Thus, in order to calculate the total uncertainty for a group of dependent calculations, the post-processing code takes the relative uncertainty calculated per run R_i from the output file and then determines the number of nonzero scores n_i it incorporates.

$$n_i = \left(\frac{1}{R_i}\right)^2 \qquad (5.9)$$

The total number of nonzero scores for all dependent calculations is then determined by summing the nonzero scores n_i for each run,

$$n = \sum_{i=1}^{I} n_i \qquad (5.10)$$

for I dependent runs.

The total relative uncertainty is then

$$R \approx \frac{1}{\sqrt{n}} \qquad (5.11)$$

which follows the general format for relative uncertainty used in LAHET and MCNP and allows us to track the precision of our measurements, until enough histories have been run that our results are statistically significant.

5.7 Summary

In this section, the foundation for a comprehensive method of performing Monte-Carlo based proton-induced neutron shielding calculations in a complex geometry has been lain. The bulk shielding structure has been successfully modeled, and software tools to read and interpret the data that the LCS provides have been developed. Preliminary testing of the tools developed in this work, including the geometry model in Section 5.2, the source term definition in Section 5.3, the materials model presented in Section 5.4, and the data interpretation techniques discussed in Section 5.5 suggest that the these tools are working properly. A comparison of predicted and measured values is presented in the following section. While a large amount of software development work and simulation time remain before the multiple source predictions of the shielding performance will be available, many of the obstacles to solving this shielding problem have been overcome. The next section will discuss a means by which the LAHET neutron dose equivalent predictions can be verified.

SECTION 6 - VERIFICATION OF CALCULATIONS

6.1 Verification of LAHET Predictions

While the LCS has been extensively and repeatedly benchmarked[44,45] at LANL and in other shielding studies,[50] calculations in a geometry of the complexity of the Northeast Proton Therapy Center have not been attempted. The LAHET simulations proposed by this work can be verified experimentally, under the same operating conditions assumed in determining the calculated values. Measurements of neutron dose equivalent rate, along with a knowledge of the beam loss configuration (i.e., the neutron source terms) are needed for this verification of the shielding performance.

The measurements may also reveal hidden flaws in the predictions, as the models may not include all of the relevant geometrical features, such as the inclusion of conduits, or of conditions that do not conform to those assumed in the construction, such as cracks or changes in the concrete density due to the absorption of water. Finally, long-term monitoring with the above measurement systems provides dose equivalent values that are based on the actual clinical workload, as opposed to the workload that was estimated for the shielding design.[7,37] Much of the data processing software for this task has already been developed at MGH and tested during the period of routine radiation protection measurements that have been performed to verify compliance with the dose restriction set by MGH and NPTC.

6.1.1 Neutron Detection Apparatus

Since the June of 1997 startup of the cyclotron at NPTC, the neutron dose equivalent rates at several locations have been monitored with a combination of thermo-luminescent dosimeters (TLD) and with up to six active neutron dose equivalent meters. The TLD's are passive dosimeters which are deployed for a period of 3 to 6 months. The

latter type of dosimeter comprises a boron trifluoride (BF_3) proportional counter, a polyethylene moderating sphere, a pulse-height discriminator and scalar, (Ludlum Measurements, Inc., Detector Model 42-31, Electronics Model 2241, Sweetwater, TX) and a personal-computer-based data acquisition system.

The boron trifluoride (BF_3) proportional counters are of a simplified Andersson-Braun (AB) type.[3] The detection mechanism of the AB counter is based on the nuclear properties of the BF_3 that fills the proportional chamber. One of the isotopes of boron, ^{10}B, has a very high thermal neutron capture cross section (3840 barns). By housing the detector within a polyethylene shell, the neutron field can be moderated, or slowed down, to thermal energies. In the $^{10}B(n,\alpha)^7Li$ reaction,(Q value=2.4 MeV, $\overline{E}_\alpha$=1.47 MeV) a thermal neutron is captured by the ^{10}B nucleus, resulting in the formation of an excited compound nucleus. This nucleus then de-excitates by the emission of an α particle, which also carries off most of the excited nucleus' energy. The deposition of the (n,α) reaction products' energy in the proportional gas registers as an electrical pulse. If that pulse is above a fixed pulse height discriminator level, it registers as a count. These counts are converted to the dose equivalent with a calibration coefficient. The associated electronics comprise a single channel analyzer for pulse height analysis, a microprocessor-controlled scalar/ratemeter/timer, and a high voltage power supply (HVPS). The meter sends the count rate to a PC via an RS-232 serial communication port. The meters have been retrofitted with bulkhead DB-9 connectors for the serial port and 3-conductor jacks. Provisions for an external 3-V power supply were added to reduce reliance on the internal battery power.

Data acquisition and online display are performed by a program written in BASIC, running on a personal computer (386 laptops, one per meter). The scalar/ratemeter transmits a stream of data to a computer and includes the count rate, scalar count, count time, and preset count time remaining. The logging program then reads and stores selected information from the stream. At 1-min intervals, a record is written to the hard disk comprising the time of day, the total scalar counts during that 1-

min interval, and the scalar counts during each 2-s subinterval of that minute. Scored over time, these counts can be converted to a dose-equivalent rate by an appropriate calibration coefficient. This calibration coefficient is determined by irradiating the meter in a known neutron calibration field.

A 5 $\pm$ 0.5 Ci (95% confidence interval) Am-Be (^{241}Am: $T_{1/2}$ = 433 y) neutron source (Amersham Corp., 5-Ci OWL Neutron Source, Model AMN.CY5, Serial No. 6829NE, Arlington Heights, IL) has been obtained to supply the calibration field. This Am-Be source provides a dose equivalent rate $\dot{H}(r_0)$ of 11.0 $\pm$ 1.1 (95% confidence interval) mrem/min/Ci at a distance r_0 of 1 m, based on a mean quality factor of 10. The calibration coefficient (C) is defined as the dose equivalent rate per scalar count rate, or

$$C = \frac{\dot{H}}{\dot{N}} \qquad (6.1)$$

Where $\dot{H}$ is the neutron dose equivalent rate at the meter and $\dot{N}$ is the count rate registered by the meter. Experimentally, this becomes

$$C = \frac{\dot{H}(r_0)(r/r_0)}{\dot{N}_{net}(r)} \qquad (6.2)$$

$$C = \frac{\dot{H}(r_0)(r/r_0)}{(\dot{N}_{tot}(r)-\dot{N}_{bkg})} \qquad (6.3)$$

where r is the distance from the source to the detector. $\dot{N}_{net}(r)$ is the net count rate at distance r, which is equal to the total count rate, $\dot{N}_{tot}(r)$ minus the average background count rate, $\dot{N}_{bkg}$.

6.1.2 Neutron Dose Equivalent Measurements

Much of the NPTC beam delivery system and beam line instrumentation has yet to be completely installed, which means that the beam intensity, beam loss locations, and other factors that influence the neutron source terms are not yet available. While these data are needed for a proper shielding study, preliminary measurements have been made in order to ensure compliance with radiation protection regulations. An example plot of the measured data used for radiation protection purposes is given in Figure 6.1. The neutron dose equivalent rate inside the accelerator vault can be multiplied by a conversion factor that incorporates a ratio between the dose equivalent rate inside the vault and the neutron dose equivalent rate on the driveway behind NPTC to constantly monitor the neutron dose equivalent in unrestricted areas, i.e., the neutron dose equivalent potentially received by members of the general public. In this case, the measurements were performed because huge gaps existed in the shielding during the construction phase, concurrent with accelerator and beamline development. This information has been used to insure that the accelerator operations at NPTC comply with regulatory limits.

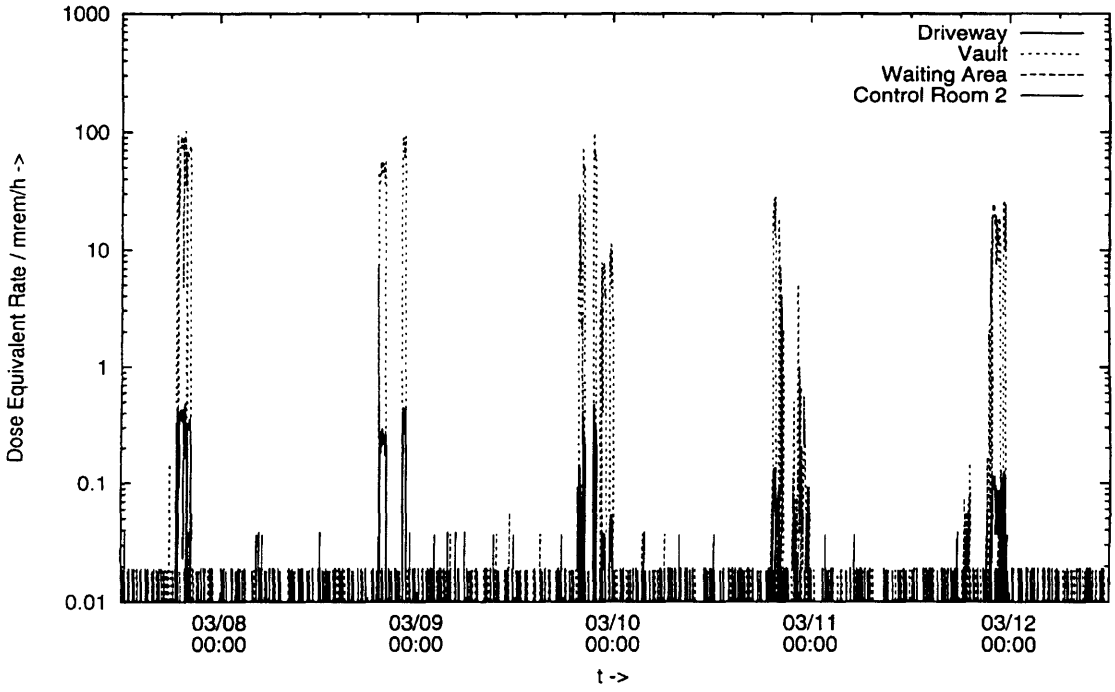

Figure 6.1. Neutron dose equivalent rates measured at several locations in the NPTC.

6.1.3 Comparison of Measurements and Calculations

Use of the neutron dose equivalent meters for radiation protection purposes has provided valuable experience not only with the detection equipment, but with the data acquisition system and post-measurement data analysis. Experimental measurements of this type are representative of the neutron dose equivalent measurements that will be physically produced during beam operation, and will be compared to the neutron dose equivalent rates predicted by the LAHET simulations. An example of this application is shown in Figure 6.2, which plots the measured neutron dose equivalent rate at several positions on the treatment floor during a period where a 10 nA ($6x10^{10}$ protons/sec) 235 MeV proton beam was deposited fully in a copper beamstop located at the isocenter of Gantry Bay 1, the first of the two primary treatment rooms. The locations of the neutron dose equivalent meters placed inside the vault, Control Room 2, and the Patient Debriefing Area are shown in Figure 6.3.

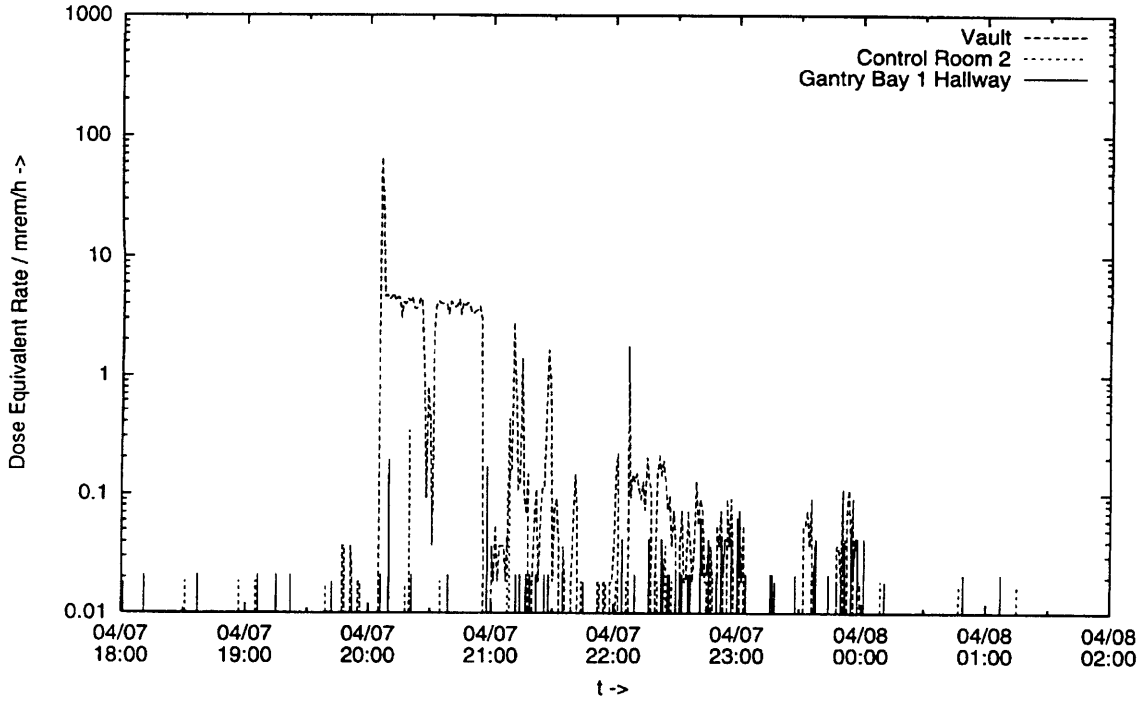

Figure 6.2. Comparison of neutron dose equivalent rates measured in NPTC at various locations.

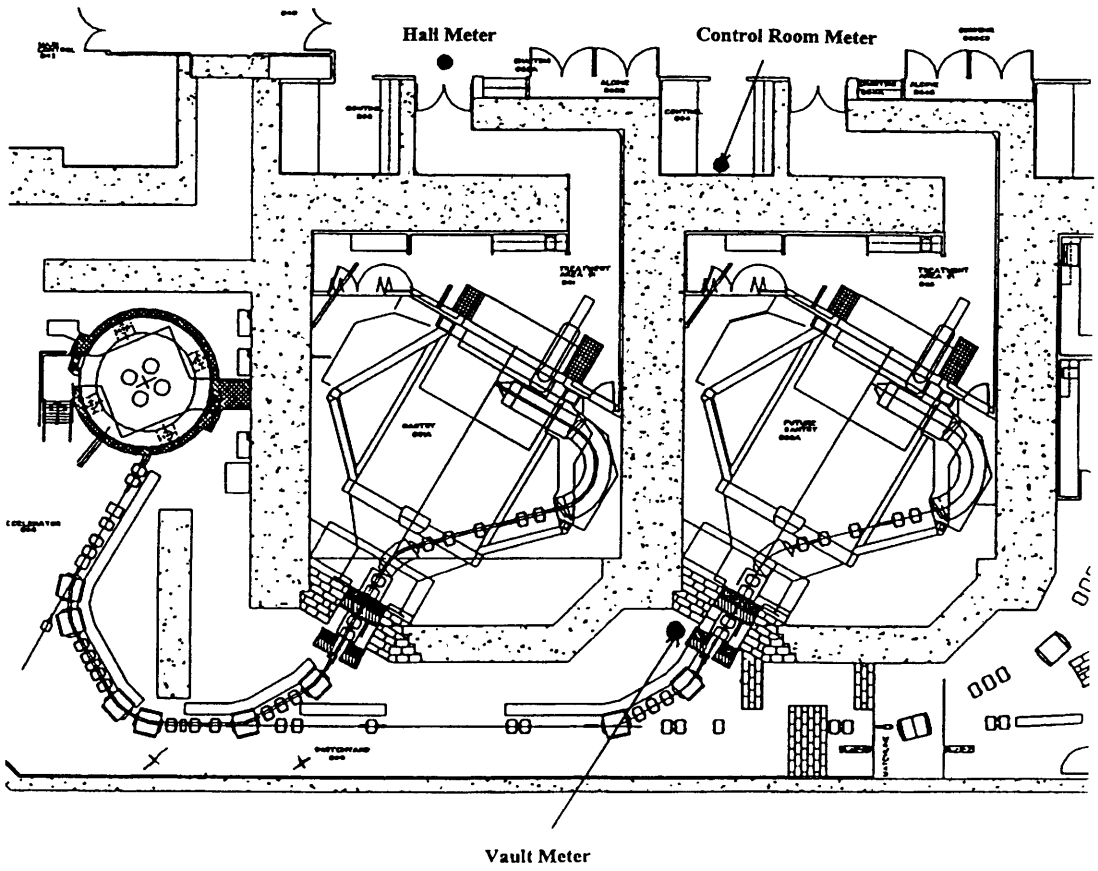

Figure 6.3. Locations of neutron dose equivalent monitoring equipment during experiment.

A summary of the measured dose rates during a 10 minute data acquisition period and the calculated dose rates for a 10 nA 235 MeV proton beam incident on a copper beamstop (see Section 5.3) is shown in Table 6.1.

Treatment Floor Position	Measured Dose Equivalent Rate (mrem/h)	Calculated Dose Equivalent Rate (mrem/h)
Outside Gantry Bay 1 Door, Hallway	0.073	0.064
Control Room 2	0.012	0.012
Inside Vault, near Gantry Bay 2 Pit	0.34	0.070

Table 6.1. Comparison of measured and calculated neutron dose equivalent rate values.

The values shown in Table 6.1 demonstrate that the values for neutron dose equivalent predicted by LAHET using the shielding geometry developed in this work agree relatively well with measured values, except for that of the accelerator vault, near the Gantry Bay 2 pit. One possible reason for this relatively large difference in predicted and measured values for the neutron dose equivalent rate is that points within the vault are relatively unshielded from neutrons produced in the accelerator housing and the beam line equipment, while the hallway and control rooms are very heavily shielded with respect to these source terms. As the only source term simulated in this preliminary study was the copper beam stop inside Gantry Bay 1, the vault values will be underpredicted while the hallway and control room 2 values will be reasonably close to the measured values. The relative uncertainties associated with these predicted values are all under 30%, which, according to the guidelines used for interpreting relative uncertainty presented by the Transport Methods Group of the Applied Theoretical and Computational Physics Division at the Los Alamos National Laboratories, can be considered reliable within a factor of two or three.[11] This relative uncertainty can be expected to improve as the number of particles simulated increases.

6.1.4 Shielding Verification

The verification of the NPTC neutron shielding using the detector and data acquisition apparatus described above is a vital task in the licensing of the facility. Using the original NPTC shielding design by Larson et al.,[28] the Bechtel Corporation calculated the neutron dose equivalent at 25 locations on the treatment floor, which are indicated by the circles in Figure 5.2 in the previous section. Those locations where personnel may face exposure to neutron radiation will be observed using the neutron dose equivalent detection and monitoring equipment described in Section 6.1.1.

One of the most important variables in the shielding verification study is where the neutrons will be produced. In the case of NPTC, this will consist of a minimum of 63

source terms, comprising 3 incident proton energies (150, 200, and 235 MeV), 3 incident proton intensities (10, 50, and 300 nA), 4 beam stop materials (graphite, iron, copper, and tissue), and a set of material-dependent beam stop locations, e.g., degrader wheel (copper and graphite), beam profile monitor (copper), 2 gantry bay entrances (copper), and 2 patients (tissue). An almost infinite number of source terms could be considered to arise from locations in the bending and focusing magnets, but these are chronic losses that cannot be rigidly controlled

Once the beamline monitoring instrumentation is fully operational, information on the proton beam characteristics will be constantly available. For a limited subset of beam operating conditions, including but not limited to beam stop location, beam stop composition, proton beam current, and incident proton energy, measurements will be made at each of the specified locations above of the neutron dose equivalent experienced at that location. In this way it can be determined if the shielding is adequate to meet the radiological safety requirements of the workers and the general public, in accordance to the limits stated in Section 3.2.3. Once a suitable set of measurements have been performed, a bank of experimental data will then be available that can be compared to each neutron dose equivalent rate calculated by LAHET for the specified tally regions. This allows for the comparison of experimental and computational results and the verification of the simulation.

6.2 Summary

A system for verifying the LAHET neutron shielding calculations while simultaneously providing an experimental means of verifying that the neutron shielding for NPTC meets the dose limits during clinical operating conditions has been provided. Six data acquisition systems have been assembled and modified in order to monitor the neutron dose equivalent during proton beam operation at several locations on a continuous basis.

SECTION 7 - CONCLUSIONS AND FUTURE WORK

7.1 Conclusions

The goal of this work was to develop improved tools for shielding calculations through the application of Monte Carlo methods in a complex, realistic geometry. In meeting this goal, the bulk shielding structure was modeled, and software tools to read and interpret the data that the LCS provides were developed. The tools developed in this work include a geometry model, a source term definition, a materials specification, and data interpretation techniques. A comparison of preliminary calculations with measurements suggests that these tools are working properly and the simulation model is valid. Neutron detection and data acquisition systems have been assembled in order to monitor the neutron dose equivalent during proton beam operation at several locations on a continuous basis, and a study implementing these data acquisition systems for verifying the LAHET neutron shielding calculations while simultaneously providing an experimental means of verifying that the neutron shielding for NPTC meets the dose limits during clinical operating conditions has been provided.

7.2 Future Work

Following the completion of the full simulation and experimental verification of the results for the Northeast Proton Therapy Center, several applications of the Monte Carlo model and the software tools developed in this work may prove viable. One such possibility would be modifications to the NPTC shielding, possibly in the form of addressing adjusted shielding requirements for increased operating capacity, or developing an optimization study of the neutron shielding for future proton therapy facilities.

7.2.1 Shielding Remediation and Modifications

If modifications need to be made to the NPTC shielding, such as the drilling of a new conduit for the purpose of running power or signal cable to a point within the shielding vault, the computer simulation shall provide us with a means by which to test such unplanned changes to the shielding before they are made. This testing will provide an idea as to what the possible radiation protection consequences of introducing a flaw into the shielding configuration might be.

If an existing shielding design proves inadequate, whether due to higher than expected patient load or unforeseen treatment configurations, it may become necessary to add additional shielding or to limit the clinical treatment load. If space or cost prohibit the installation of additional shielding, some adjustment to the treatment load may become necessary. As will be described in Section 7.2.2, one could optimize the patient treatment configurations without making changes in the shielding design. Use of such a simulation will also allow for the design and testing of localized shielding around established neutron sources, which will also allow for reduction of the dose equivalent rates outside the shielding without any further modification to the bulk shielding structure.

The simulation tools will allow us to test alternative shielding materials in order to reduce their cost and size. Computer simulations may also facilitate the testing of beam line materials that optimize beam quality for treatment while minimizing this neutron production. In the case of NPTC, the simulation could also provide for an optimized shielding design for a third gantry treatment room. A rigorous computer aided design may allow us to build the third treatment room with less shielding, making its construction a more financially viable option, with the potential of increasing the clinical capacity of the facility.

7.2.2 Shielding Optimization

In order to utilize the Monte Carlo model developed for NPTC to optimize neutron shielding in new facilities, a system by which to iteratively determine the "best" design must be integrated. While case-by-case improvements on specific problem areas requires comparatively little computer time, they are inefficient in the long term in that they are based on educated guesses. Numerical optimization algorithms may offer an alternative approach to optimizing neutron shielding design. There are two basic means by which to obtain the optimum shielding solution: one is to vary the barrier thickness for some fixed set of operating conditions, the other is to vary the operating conditions for a given set of shielding barrier thicknesses. The former is the approach to be used for designing new facilities, and the latter may provide an economical remedial solution if deficiencies in the shielding appear, whether due to a flaw in the original shielding design or changes in the patient treatment load or configuration. For optimization work, the cost variable as a function of barrier thickness will be minimized while the dose equivalent rates are constrained to the specified dose limits where the facility is to be constructed. Care must be taken, however, that the optimization configuration determined is a true global optimum, rather than a local optimum that does not reflect on the shielding needs of the entire facility.

WORKS CITED

1. AGOSTEO, S., ARDUINI, G., BODIE, G., MONTI, S., PADOANI, F., RINDI, A., SILARI, M., TINTI, R., TROMBA, G., Shielding Calculations for a 250 MeV Hospital-Based Proton Accelerator, Hadrontherapy Centre, Italy (1995).

2. ALSMILLER, R.G., SANTORO, R.T., BARISH, J., Shielding Calculation for a 200 MeV Proton Accelerator and Comparisons with Experimental Data, Particle Accelerators **7** (1975).

3. ANDERSSON, I.O., BRAUN, J., A Neutron Rem Counter, Nukleonik **6**, (1964).

4. BERTINI, H.W., Low energy intranuclear cascade calculations, Physics Review **131** (1963) 1801.

5. BERTINI, H.W., Preliminary Data from Intranuclear Cascade Calculations of 0.75, 1, and 2 GeV Protons on Oxygen, Aluminum, and Lead, and 1 GeV Neutrons on the Same Elements, Rep. ORNL-TM-1996, Oak Ridge National Laboratory, Oak Ridge, TN (1967).

6. BERTINI, H.W., Intranuclear cascade calculation of the secondary nucleon spectra from nucleon-nucleus interactions in the energy range 340-2900 MeV and comparison with experiment, Physics Review **188** (1969) 1711.

7. BECHTEL CORPORATION, Program of Requirements, Safety and Security, Northeast Proton Therapy Center, Massachusetts General Hospital, August 26 (1994).

8. BRENNER, D.J., PRAEL, R.E., DICELLO, J.F., ZAIDER, M., Improved Calculations of Energy Deposition from Fast Neutrons, (Proceedings of the Fourth Symposium on Neutron Dosimetry) EUR-7448, Munich-Neuherberg (1981).

9. BRAID, T.H., RAPIDS, R.F., SIEMSSEN, R.H., TIPPIE. J.W., O'BRIEN, K., Calculations of Shielding for Large Cyclotrons, IEEE Trans. Nucl., Sci., **NS-18**, (1971) 824.

10. BRENNER, D.J., PRAEL, R.E., Calculated Differential Secondary-Particle Production Cross-Sections after Nonelastic Neutron Interactions with Carbon and Oxygen between 10 and 60 MeV, Atomic and Nuclear Data Tables **41**, (1989) 71-130.

11. BRIESMEISTER, J., MCNP - A General Monte Carlo N-Particle Transport Code, Version 4B, Report LA-7396-M Revised, Los Alamos National Laboratory, (1997).

12. CHEN, K., FRAENKEL, Z., FRIEDLANDER, G. GROYER, J.R., MILLER, J.M., SHIMAMOTO, Y., VEGAS: A Monte Carlo simulation of intranuclear cascades, Physics Review **166** (1968) 949.

13. CLOVER, M.R., DEVRIES, R.M., DIGIACOMO, N.J., YARIV, Y., Physics Review C **26**, (1982) 2138.

14. COLE, F.T., Accelerator Considerations in the Design of a Proton-Therapy Facility - A Reprise, Particle Accelerator Corporation, 4513 Cornell Avenue, Downers Grove IL 60515, [Aug. 31 1991].

15. COLEMAN, W.A., Thermal-Neutron Flux Generation by High-Energy Protons, Report ORNL-TM-2206, Oak Ridge National Laboratory, Oak Ridge, TN, (1968).

16. de STAEBLER, H., Transverse Shielding for the Stanford Two-Mile Accelerator, Report SLAC-9, Stanford Linear Accelerator Center, CA (1962).

17. de STAEBLER, H., Average Radiation Levels Inside the Accelerator Housing When the Machine is Off, Report SLAC-9, Stanford Linear Accelerator Center, CA (1962).

18. GUTHRIE, M.P., EVAP-4: Another Modification of a Code to Calculate Particle Evaporation from Excited Compound Nuclei, Report ORNL-TM-3119, Oak Ridge National Laboratory, Oak Ridge, TN (1970).

19. HARDER, D., Recently proposed concepts and quantities in radiation protection, Report EUR-7101-EN, Harwood Academic Publishers, Chur, Switzerland (1981) 15.

20. INTERNATIONAL COMMISSION ON RADIOLOGICAL PROTECTION, Data for Protection Against Ionizing Radiation from External Sources, Supplement to ICRP Publication 15, ICRP Publication 21, Pergamon Press, Oxford and New York (1973).

21. INTERNATIONAL COMMISSION ON RADIOLOGICAL PROTECTION, Recommendations of the ICRP, ICRP Publication 26, Pergamon Press, Oxford and New York (1977).

22. INTERNATIONAL COMMISSION ON RADIOLOGICAL PROTECTION, General Principles of Monitoring for Radiation Protection of Workers, ICRP Publication 35, Pergamon Press, Oxford and New York (1982) para. 5.

23. INTERNATIONAL COMMISSION ON RADIOLOGICAL PROTECTION, The Value of the Quality Factor in the Case of Neutrons, Statement from the 1985 Paris Meeting of the ICRP, ICRP/85/G-03 (1985).

24. INTERNATIONAL COMMISSION ON RADIATION UNITS AND MEASUREMENTS, Radiation Quantities and Units, ICRP Report 11, Washington, DC (1968).

25. INTERNATIONAL COMMISSION ON RADIATION UNITS AND MEASUREMENTS, Quantities and Units in Radiation Protection and Dosimetry, ICRP Report 51, Washington, DC (1968).

26. ION BEAM APPLICATIONS, Louvain-la-neuve, Belgium (1998).

27. IRVING, D.C., FREESTONE, R.M. Jr., KAM, F.B.K., O5R, A General Purpose Monte Carlo Neutron Transport Code, Report ORNL-3622, Oak Ridge National Laboratory, Oak Ridge, TN (1965).

28. LARSON, A., et al., Northeast Proton Therapy Center Shielding Design Description, Bechtel Corporation, 10 August, 1995.

29. LOEFFLER, J.S., SMITH, A.R., SUIT, H.D., The Potential Role of Proton Beams in Radiation Oncology, Seminars in Oncology, **24** 6 (1997).

30. LUNDQVIST, H., Radiation Protection Calculations for a Proton Cyclotron in the Energy Range 100-400 MeV, Dept. of Radiobiology, Gustaf Werner Institute, University of Uppsala, Sweden, Report GWI-R 18/72 (1972).

31. MAYO, C., KOEHLER, A., GOTTSCHALK, B., GALL, K., Recommendations for Neutron Radiation Shielding Parameters Used in the Design of a Proton Medical Facility, HCL Note, April 16 (1993).

32. McCASLIN, J.B., SMITH, A.R., CHEN, G.T., ZNK, S., Absorbed Dose Estimates of Neutrons from the Primary Beam Particle Interactions in a Water Phantom at the 184-Inch Synchrocyclotron Medical Facility, Report HPN-142, Lawrence Berkeley Laboratory, Berkeley, CA (1984).

33. McCRACKEN, D.D., The Monte Carlo Method, Scientific American **192**, (1955) 90.

34. METROPOLIS, N., BIVINS, R., STORM, M., TURKEVITCH, A., MILLER, J.M., FRIEDLANDER, G., Monte Carlo calculations of intranuclear cascades, Physics Review **110** (1958) 185.

35. NATIONAL COUNCIL ON RADIATION PROTECTION AND MEASUREMENTS, Protection Against Neutron Radiation, NCRP Publication 38 (1971).

36. NEWHAUSER, W.D., ROSS, M.A., HSU, H.H., A Primer on Solving Dosimetry Problems with LAHET, Northeast Proton Therapy Center Report 98-01, 26 Sept. 1997.

37. NPTC SAFETY COMMITTEE, Radiation Shielding Guidelines for the Northeast Proton Therapy Center. NPTC Report NPTC 11, 10 Feb., 1993.

38. ORTHEL, J.L., KNOWLES, H.B., HILL, B.W., Final Report for the LBL/UCDMC Proton Treatment Facility Shielding and Activation Study, Contact DE-ADC03-76SF00098, Lawrence Berkeley Laboratory, Feb. 26 (1993).

39. PARKER, H.M., Health Physics, Instrumentation, and Radiation Protection, Advances in Biology and Medical Physics **1** (1948) 223.

40. PATTERSON, H.W., LOW-BEER, A.G., SARGENT, T.N., Whole-body counting and bioassay determination of accelerator workers, Health Physics **17** (1969) 621.

41. PERSLIDEN, J., Application of the Monte Carlo Method to Diagnostic Radiology, Linkoping University Medical Dissertations, Linkoping, Sweden **20** (1986).

42. PRAEL, R.E., BOZOIAN, M., Adaptation of the Multistage Preequilibrium Model for the Monte Carlo Method (I), Report LA-UR-88-3238, Los Alamos National Laboratory. September (1988).

43. PRAEL, R. E., LICHTENSTEIN, H., User Guide to LCS: The LAHET Code System, Report LA-UR-89-3014, Los Alamos National Laboratory (1989).

44. PRAEL, R.E., LAHET Benchmark Calculations of Differential Neutron Production Cross Sections for 113 MeV and 256 MeV Protons, Report LA-UR-89-3347, Los Alamos National Laboratory, September (1989).

45. PRAEL, R.E., The LAHET Code System: Introduction, Development, and Benchmarking, (Proceedings of the Workshop on Simulating Accelerator Environments) Report LA-12835-C, Los Alamos National Laboratories, Santa Fe, NM (1993) 204.

46. PRAEL, R.E., Upgrade Package for LCS with LAHET 2.7, Report LA-UR-97-4981, Los Alamos National Laboratory, Dec. 1 (1997).

47. PUPPI, G., DALLAPORTA, N., "The equilibrium of the cosmic ray beam in the atmosphere," Progress in Cosmic Ray Physics (WILSON, J.G., Ed.), Vol. 1 (1965) 317.

48. RADIATION SHIELDING INFORMATION CENTER, HETC Monte Carlo High-Energy Nucleon-Meson Transport Code, Report CCC-178, Oak Ridge National Laboratory, August (1977).

49. ROSSI, H., WAMBERSIE, A., ET AL., Clinical Proton Dosimetry Part 1: Beam Production, Beam Delivery and Measurement of Absorbed Dose, RC on Proton Dosimetry (1996).

50. SIEBERS, J.V., Shielding Measurements for a 230 MeV Proton Beam, University of Wisconsin, Ph. D. dissertation, 1990.

51. SMITH, A.R. , SCHIMMERLING, W. KANSTEIN, L.L., McCASLIN, J.B., THOMAS, R.H., Neutron flux density and secondary-particle energy spectra at the 184-Inch Synchrocyclotron Medical Facility, Medical Physics **8** 5 (1981) 668.

52. SUIT, H.D., URIE, M., EFIRD, J.T., Proton Beams in Clinical Radiation Therapy, Principles and Practice of Oncology, **6** (1992).

53. SWANSON, W.P., Estimate of the risk in radiation therapy due to unwanted neutrons, Medical Physics **7** 2 (1980) 141.

54. TESCH, A., A simple estimation of the lateral shielding for proton accelerators in the energy range from 50 to 1000 MeV, Radiation Protection and Dosimetry **11** 3 (1985) 165.

55. THOMAS, R.H., STEVENSON, G.R., Radiation protection around high-energy accelerators, Radiation Protection and Dosimetry **10** 1-4 (1985) 283.

56. THOMAS, R.H., "Dosimetric Aspects," Some Important Issues in Developing Radiation Protection Issues (Proceedings of the 1984 Annual Meeting of the National Council on Radiation Protection and Measurements, Washington, DC) NCRP, Washington , DC (1985) 182.

57. THOMAS, R.H., STEVENSON, G.R., Radiological Safety Aspects of the Operation of Proton Accelerators, International Atomic Energy Agency Technical Reports Series No. 283, Vienna (1988).

58. UNITED STATES NUCLEAR REGULATORY COMMISSION, Standards for Protection Against Radiation, Title 10, Chapter 1, Part 20 (1995).

59. VAN RIPER, K.A., SABRINA User's Guide, Report LA-UR-93-3696, Los Alamos National Laboratory, October (1993).

60. WAGNER, S.R., Quantities and units for neutron dosimetry in radiation protection, Radiation Protection and Dosimetry, **10** 1-4 (1985) 23.

61. WILSON, R.R., Radiological Use of Fast Protons, Radiology **47** (1946).

62. YARIV, Y., FRAENKEL, Z., Physics Review C **20** (1979) 2227.

63. YARIV, Y., FRAENKEL, Z., Physics Review C **24** (1981) 488.

64. ZAZULA, J.M., TESCH, K, Nucl. Instrum. Meth. A **288** (1990) 279-294.

65. ZHOU, X.L., Principles of Radiation Applications for Medicine and Industry, 22.55 Lecture Notes, Massachusetts Institute of Technology, Cambridge (1998).

APPENDIX

Section 1. Isotopic abundances of materials used in the simulation.

Isotope	Mass [amu]	Percent Abundance	Mass Fraction	ρ [A^3]	ρ [g/cc]
H-1	1.007825	99.985	0.100970	6.7572E-02	1.1309E-01
H-2	2.014102	0.015	0.000030	1.0000E-05	3.4000E-05
H-nat	1.007976	100	0.101000	6.7582E-02	1.1321E-01
C-12	12.000000	98.9	0.767633	4.3147E-02	8.5978E-01
C-13	13.003355	1.1	0.009337	4.8400E-04	1.0458E-02
C-nat	12.011137	100	0.777000	4.3631E-02	8.7024E-01
O-16	15.994915	99.76	0.051860	2.1868E-03	5.8083E-02
O-17	16.999131	0.038	0.000021	8.3298E-07	2.3514E-05
O-18	17.999160	0.204	0.000119	4.4718E-06	1.3366E-04
O-nat	15.999705	100	0.052000	2.1921E-03	5.8240E-02
N-14	14.003074	99.63	0.034863	1.6792E-03	3.9046E-02
N-15	15.000109	0.366	0.000137	6.1686E-06	1.5400E-04
N-nat	14.006163	100	0.035000	1.6854E-03	3.9200E-02

Table A.1. Isotopic masses, abundances, mass fractions, and densities in A-150 tissue equivalent plastic. (ρ=1.127 g/cc)

Isotope	Mass [amu]	Percent Abundance	Mass Fraction	ρ [A^3]	ρ [g/cc]
Cu-63	62.929599	69.2	0.685298	5.8628E-02	6.1266E+00
Cu-65	64.927793	30.8	0.314702	2.6094E-02	2.8134E+00
Cu-nat	63.545403	100	1.000000	8.4722E-02	8.9400E+00

Table A.2. Isotopic masses, abundances, mass fractions, and densities in copper. (ρ=8.94 g/cc)

Isotope	Mass [amu]	Percent Abundance	Mass Fraction	ρ [A^3]	ρ [g/cc]
C-12	12.000000	98.9	0.987983	8.4286E-02	1.6796E+00
C-13	13.003355	1.1	0.012017	9.4600E-04	2.0429E-02
C-nat	12.011137	100	1.000000	8.5233E-02	1.7000E+00

Table A.3. Isotopic masses, abundances, mass fractions, and densities in graphite. (ρ=1.7 g/cc)

Isotope	Mass [amu]	Percent Abundance	Mass Fraction	ρ [A^3]	ρ [g/cc]
H-1	1.007825	99.985	0.000000	0.0000E+00	0.0000E+00
H-2	2.014102	0.015	0.000000	0.0000E+00	0.0000E+00
H-nat	1.007976	100	0.000000	0.0000E+00	0.0000E+00
C-12	12.000000	98.9	0.000123	7.4083E-09	1.4762E-07
C-13	13.003355	1.1	0.000001	8.3155E-11	1.7956E-09
C-nat	12.011137	100	0.000124	4.3631E-02	1.4942E-07
O-16	15.994915	99.76	0.231155	1.0487E-05	2.7854E-04
O-17	16.999131	0.038	0.000094	3.9946E-09	1.1276E-07
O-18	17.999160	0.204	0.000532	2.1445E-08	6.4097E-07
O-nat	15.999705	100	0.231781	1.0512E-05	2.7930E-04
N-14	14.003074	99.63	0.752307	3.8985E-05	9.0653E-04
N-15	15.000109	0.366	0.002960	1.4322E-07	3.5673E-06
N-nat	14.006163	100	0.755267	3.9128E-05	9.1010E-04
F-nat	18.998403	100	0.017000	6.4932E-07	2.0485E-05
Ar-36	35.967546	0.337	0.000039	7.8523E-10	4.6899E-08
Ar-38	37.962000	0.063	0.000566	1.3337E-09	8.4072E-08
Ar-40	39.962000	99.6	0.942020	2.1984E-06	1.3992E-04
O-nat	39.942000	100	0.231781	2.1106E-06	1.4005E-04

Table A.4. Isotopic masses, abundances, mass fractions, and densities in air. (ρ=1.23E-3 g/cc)

Isotope	Mass [amu]	Percent Abundance	Mass Fraction	ρ [A^3]	ρ [g/cc]
H-1	99.985	99.985	0.005998	1.0150E-02	1.6987E-02
H-2	0.015	0.015	0.000002	1.5227E-06	5.0929E-06
H-nat	100	100	0.006000	1.0152E-02	1.6992E-02
C-12	12.000000	98.9	0.152149	2.1623E-02	4.3089E-01
C-13	13.003355	1.1	0.001851	2.4271E-04	5.2409E-03
C-nat	12.011137	100	0.154000	2.1866E-02	4.3613E-01
O-16	15.994915	99.76	0.356037	3.7962E-02	1.0083E+00
O-17	16.999131	0.038	0.000144	1.4460E-05	4.0819E-04
O-18	17.999160	0.204	0.000819	7.7628E-05	2.3202E-03
O-nat	15.999705	100	0.357000	3.8054E-02	1.0110E+00
Mg-24	23.985042	78.99	0.021046	1.4965E-03	5.9604E-02
Mg-25	24.985837	10	0.002776	1.8945E-04	7.8606E-03
Mg-26	25.982594	11.01	0.003178	2.0859E-04	8.9997E-03
Mg-nat	24.302421	100	0.027000	1.8945E-03	7.6464E-02
Si-28	27.976927	92.23	0.172722	1.0529E-02	4.8915E-01
Si-29	28.976495	4.67	0.009058	5.3312E-04	2.5653E-02
Si-30	29.973770	3.1	0.006220	3.5389E-04	1.7615E-02
Si-nat	28.085509	100	0.188000	1.1416E-02	5.3242E-01
Ca-40	39.963591	96.94	0.259044	1.1055E-02	7.3361E-01
Ca-42	41.958618	0.647	0.001815	7.3783E-05	5.1409E-03
Ca-43	42.958766	0.135	0.000388	1.5395E-05	1.0982E-03
Ca-44	43.955481	2.09	0.006143	2.3834E-04	1.7397E-02
Ca-46	45.953689	0.0035	0.000011	3.9913E-07	3.0458E-05
Ca-48	47.952533	0.187	0.000600	2.1325E-05	1.6981E-03
Ca-nat	40.080120	100	0.268000	1.4040E-02	7.5898E-01

Table A.5. Isotopic masses, abundances, mass fractions, and densities in concrete. (ρ=2.832 g/cc)